isvr Institute of Sound and Vibration Research

Nonlinear Vibration of Plates by the Hierarchical Finite Element and Continuation Methods

P.M.L. Ribeiro and M. Petyt

ISVR Technical Memorandum 821

July 1997

University of Southampton

SCIENTIFIC PUBLICATIONS BY THE ISVR

Technical Reports are published to promote timely dissemination of research results by ISVR personnel. This medium permits more detailed presentation than is usually acceptable for scientific journals. Responsibility for both the content and any opinions expressed rests entirely with the author(s).

Technical Memoranda are produced to enable the early or preliminary release of information by ISVR personnel where such release is deemed to the appropriate. Information contained in these memoranda may be incomplete, or form part of a continuing programme; this should be borne in mind when using or quoting from these documents.

Contract Reports are produced to record the results of scientific work carried out for sponsors, under contract. The ISVR treats these reports as confidential to sponsors and does not make them available for general circulation. Individual sponsors may, however, authorize subsequent release of the material.

UNIVERSITY OF SOUTHAMPTON

INSTITUTE OF SOUND AND VIBRATION RESEARCH

STRUCTURAL DYNAMICS GROUP

Nonlinear Vibration of Plates by the Hierarchical Finite Element and Continuation Methods

by

P.M.L. Ribeiro and M. Petyt

ISVR Technical Memorandum No. 821

July 1997

Authorized for issue by
Dr. R.J. Pinnington
Group Chairman

CONTENTS

LIST OF TABLES

LIST OF FIGURES

ABSTRACT

In this technical memorandum the hierarchical finite element (HFEM) and harmonic balance methods are applied to derive the equations of motion of thin, isotropic and symmetric laminated plates vibrating with large amplitude displacements. Symbolic computation is used in the derivation of the model. Free and steady-state forced vibration with large amplitude displacements are studied. The equations of motion are solved by the Newton and continuation methods. The stability of the obtained solutions is investigated by Floquet's theory. The convergence properties of the HFEM, the influence of the number of degrees of freedom and of in-plane displacements are discussed, as well as the capabilities of the numerical methods presented. The HFEM results are compared with published experimental and numerical results and good agreement is found.

1 INTRODUCTION

For many practical and engineering purposes, problems in structural dynamics are solved using linear theories. However, the solutions obtained based on linear models are known to be just a first approximation to the actual solutions. If a structure vibrates with large amplitudes, linearized models become inadequate.

As the excitations to which structures are subjected increased and their weight decreased, large vibration amplitudes became more frequent. They occur, for example, in aeronautic, naval and aerospace structures. Particularly in the aircraft industry, greater performance capabilities resulted in greater acoustic and aerodynamic excitation levels. On the other hand, there is a frequent use of thin-walled structural components in the design of aircrafts [41]. As a result, large amplitude, geometrically non-linear vibration of the aircraft skin-panels, and consequently reduced fatigue life, may occur.

The effect of geometric nonlinearity on plates with fixed ends is of the hardening spring type, i.e., the "resonance frequency" increases with the amplitude of vibration. The "mode shape" changes during the "period of vibration" and is amplitude dependent [2, 3, 14, 15]. For structures under harmonic excitation, sub- and superharmonic [48], quasi periodic and chaotic responses [22, 27] are possible.

There is an interest in developing models more realistic than the linear ones and many researchers and engineers abandoned the linear theories in favour of nonlinear methods of solution. Mathematical models have been developed for predicting the nonlinear behaviour of structures. These models involve nonlinear equations, whose solution frequently can only be obtained approximately and iteratively. A reformulation of the nonlinear stiffness matrix should be carried out in each iteration, until convergence is achieved. The superposition principle is not applicable in nonlinear problems. Consequently, the nonlinear dynamic analysis is much more complicated than the linear one and the time needed to solve the model increases very much with the number of

degrees of freedom (DOF). In order to overcome this, assumptions are usually made, which inevitably affect the accuracy of the solution. Some approaches are based on single-mode analysis [6, 40, 44]. Other approaches, when the structure under study is a plate, are based on Berger's hypothesis [5]. According to this hypothesis the effect of the strain energy due to the second invariant of the strains in the middle surface of the plate is neglected; that is, the sum of the in-plane forces (N_1+N_2) is assumed to be constant in the middle surface of the entire plate.

The development of more powerful computers and computational methods enabled researchers to solve the non-linear models more accurately. In particular, the finite element method (FEM) has been extensively applied in the nonlinear analysis of plates. Mei [23] was one of the first to study the free vibrations of isotropic plates by the FEM, assuming that the in-plane forces were constant within each plate element, but could vary from element to element. Rao et al. [32] made no assumption about the variation of the in-plane forces in each element, neglected the in-plane displacements and linearized the von Kármán nonlinear membrane strain terms. The motion was assumed to be harmonic. Reddy & Chao [34] presented an element based on von Kármán large deflection theory but including transverse shear and large rotations. Lau et al. [18, 19] developed a triangular element, including in-plane displacements and carried out free and forced vibration analysis. The HBM (harmonic balance method) was applied; the consideration of two harmonics in the time function lead to the discovery of internal resonances. Mei & Decha-Umphai [24], presented a finite element for the large amplitude vibration of thin plates subjected to harmonic loading. A linearizing function was used to linearize the strain energy. The equation of motion was transformed into an eigenvalue problem by using a harmonic force matrix. Rao, Sheikh & Mukhopadhyay [33] applied an isoparametric element with eight nodes and five degrees of freedom per node, to study large free vibration of plates and of stiffened plates; von Kármán's equations were adopted and in-plane deformation and inertia were taken into account. Benamar et al. [3] assumed harmonic motion and expanded

the transverse displacement in the form of a finite series of functions, to derive the strain and kinetic energies. In-plane displacements, transverse shear and rotatory inertia were neglected. The same authors, in a later work [4], presented a set of experiments carried out in order to investigate the dynamic response of fully clamped plates. It was confirmed that the slope of the "mode shape" near the clamps and the frequency of vibration increase with the amplitude of vibration.

The works referred to previously are about plates constructed in isotropic materials. Although composite materials have been used for centuries, it is in the recent past that their use has increased considerably. High stiffness and strength, low thermal expansion, minimum weight and other properties may be achieved by combining different materials together. Through variation of the fibber orientation and stacking sequence, laminated composite plates can be tailored so that their strength and stiffness matches the loading environmement. Composite panels are used in commercial and military aircraft, missiles, ships, automobiles and several other industries [42]. In many of these applications, dynamic external excitations are of a very high level, causing geometrical nonlinearity. Compared to isotropic plates, the geometrical nonlinear vibration analysis of laminated plates is more complex, due to the anisotropic material properties, the lower transverse shear strength and elastic shear modulus, the coupling between bending and twisting deformations and between bending and stretching deformations.

Nonlinear vibration of laminated plates has received much attention. A review on the work done in this field, prior to 1988 can be found in [7]. Prabhakara & Chia [30] presented an analytical multi-mode approach of free flexural vibrations of orthotropic plates. The HBM method was used. It was found that the accuracy of the single mode approach decreases with increasing amplitudes of vibration, and that this effect is more significant for orthotropic than for isotropic plates. Singh et al. [43] proposed a method of direct numerical integration of the frequency-ratio expression to study non-linear free vibration of rectangular cross-ply plates. Ganapathi et al. [10] used an element

with eigth nodes and five nodal degrees of freedom to study free vibrations of laminated plates. Prathap & Varandan's [31] reinterpretation of frequency for nonlinear vibrations was followed and the governing equations were solved for the point of reversal of motion. Chiang et al. [8] developed a rectangular element with 24 DOF to determine the large amplitude free and steady-state vibration responses of laminated composite plates. The HBM and an iterative correction procedure to obtain the "mode shape" were applied. Woo & Nair [52] used von Kármán's assumption and Galerkin's method to derive the equations of motion of laminated plates in free non-linear vibration. These equations were solved with the help of the HBM and a modified Newton-Raphson algorithm. The results were compared with direct numerical integration of sixth order Runge-Kutta-Verner. Sarma et al. [38, 39] studied free vibration of thin laminated plates. The equations of motion were derived from energy functions, applying Hamilton's principle.

It is known that, in linear problems, the hierarchical finite element method (HFEM) tends to give accurate results with fewer DOF than the *h*-version of the FEM [1, 12, 13, 26]. In the HFEM, better approximations are accomplished by adding higher order shape functions to the existing model, without redefining the mesh. The linear matrices possess the embedding property, i.e., the associated element matrices for a number of shape functions $p=p_1$ are always submatrices for $p=p_2$, $p_2 \geq p_1$. The existing nonlinear matrices of an approximation of lower order, p_1, can be used in the derivation of the nonlinear matrices of the improved approximation, p_2. This method provides a very flexible choice in selecting the number of DOF according to the problem analysed and accuracy required. In order to reduce the number of DOF, Han & Petyt [11, 14, 15] applied the HFEM to study the free vibration of isotropic and laminated plates with geometrical non-linearity. Von Kármán's nonlinear strain-displacement relationship was employed. The in-plane displacements were included in the model. The stiffness and mass matrices present in the equations of motion were developed by applying the principle of virtual work. Using the

HBM equations in the frequency domain were derived; these equations were solved by an iterative numerical procedure. The use of very high-order polynomial displacement shape functions made it possible to model the whole rectangular plate with only one element and to obtain accurate results with a small number of degrees of freedom. The first three modes of vibration were analysed.

In nonlinear vibrations, the frequency response (FRF) and the backbone curves can have multi-valued regions, turning and bifurcation points. Therefore, their complete and automatic description is not easy, or even possible, by using the Newton or other simple iterative methods. In beam vibration analysis this problem was successfully overcome by apllication of a continuation method [20, 36, 37].

In this report the HFEM will be used to model thin, rectangular, isotropic and laminated fully clamped plates as in references [11], [14] and [15]. The case of fully clamped boundaries can be adequate for idealising many real panel-type situations, such as aircraft wing panels [47]. Although the HFEM has already been applied to study geometrical nonlinear free vibration, difficulties were encountered in achieving convergence for large amplitudes of vibration [11]. By applying the continuation method these difficulties can be overcome. The HFEM will be applied, to the authors best knowledge for the first time, to study steady-sate forced vibration of plates with geometrical nonlinearity. The excitations considered will be harmonic plane acoustic waves at normal and grazing incidence, which are assumed to represent aerodynamic forces or jet-engine noise. The vector of external forces is modelled using the principle of virtual work. The time variation of the solution is going to be expressed by means of a Fourier series and the harmonic balance method will be applied. The stability of the steady-state solutions will be studied by Floquet's theory.

Authors generally restrain their numerical analysis to the first mode. In this report, free and steady state forced vibration around higher order modes will be analysed by taking advantage of the small number of DOF required in the HFEM model.

2 MATHEMATICAL MODEL

2.1 *Hierarchical finite element model*

The analysed plates are assumed to be elastic, with thin uniform thickness h. Laminated plates are constituted of homogeneous and orthotropic layers, with uniform thickness and perfectly bonded together.

Following Kirchhoff's hypothesis, tractions on surfaces parallel to the reference plane are considered to be negligibly small when compared with the inplane stresses, the effect of the transverse shear deformation is neglected and the inplane displacements are linear functions of z [6]. The effect of transverse shear deformation is more important in composite than in isotropic plates, because of their low shear modulus. According to Mei & Prasad [25], the effects of transverse shear deformation in symmetrically laminated composite plates can be neglected when the span to thickness ratio is $a/h > 50$. Applying Kirchhoff's hypothesis, the inplane displacements u and v, and the transverse deflection at any point of the plate are given by:

$$\begin{aligned} u(x,y,z,t) &= u^0(x,y,t) - zw^0_{,x} \\ v(x,y,z,t) &= v^0(x,y,t) - zw^0_{,y} \\ w(x,y,z,t) &= w^0(x,y,t) \end{aligned} \qquad (2.1)$$

where $,x$ denotes differentiation with respect to x; u^0, v^0 and w^0 are the values of u, v and w in the reference plane, which is the middle plane. Equations (2.1) are those of von Kármán.

The rotatory inertia will also be neglected. Its effect is smaller than the effect of transverse shear deformation and can be neglected for most engineering applications [6].

The von Kármán nonlinear strain displacement relationships are

$$\begin{aligned}\varepsilon_x &= \varepsilon_x^{\,0} + z\kappa_x \\ \varepsilon_y &= \varepsilon_y^{\,0} + z\kappa_y \\ \gamma_{xy} &= \gamma_{xy}^{\,0} + z\kappa_{xy}\end{aligned} \tag{2.2}$$

where $\varepsilon_x^{\,0}$, $\varepsilon_y^{\,0}$ and $\gamma_{xy}^{\,0}$ are the in-plane strain components at $z = 0$ defined by

$$\varepsilon_x^0 = u_{,x} + \frac{1}{2}w_{,x}^2,\ \varepsilon_y^0 = v_{,y} + \frac{1}{2}w_{,y}^2,\ \gamma_{xy}^0 = u_{,y} + v_{,x} + w_{,x}w_{,y}, \tag{2.3}$$

and κ_x, κ_y and κ_{xy} are the plate curvatures given by

$$\kappa_x = -w_{,xx},\ \kappa_y = -w_{,yy},\ \kappa_{xy} = -2w_{,xy}. \tag{2.4}$$

For each element, the middle plane displacements (Figure 1) are expressed in the form:

$$\begin{Bmatrix} u_0 \\ v_0 \\ w_0 \end{Bmatrix} = [N]\begin{Bmatrix} q_p \\ q_w \end{Bmatrix} \tag{2.5}$$

$$[N] = \begin{bmatrix} \lfloor N^u \rfloor & 0 & 0 \\ 0 & \lfloor N^u \rfloor & 0 \\ 0 & 0 & \lfloor N^w \rfloor \end{bmatrix} \tag{2.6}$$

$$\lfloor N^u \rfloor = \lfloor g_1(\xi)g_1(\eta) \quad g_1(\xi)g_2(\eta) \cdots g_{p_i}(\xi)g_{p_i}(\eta) \rfloor \tag{2.7}$$

$$\lfloor N^w \rfloor = \lfloor f_1(\xi)f_1(\eta) \quad f_1(\xi)f_2(\eta) \cdots f_{p_o}(\xi)f_{p_o}(\eta) \rfloor \tag{2.8}$$

Where p_o and p_i are the number of out-of-plane and of in-plane shape functions used in the model; $\{g\}$ and $\{f\}$ are the vectors of in- and out-of-plane shape functions; q_p and q_w are the generalised in- and out-of-plane displacements and $[N]$ the matrix of shape functions. The set of shape functions used is the Rodrigues' form of Legendre polynomials [11].

Since one element, or "super-element", will prove to be enough to study the vibration of the plates considered in this report, the local and global coordinates are related by:

$$\xi = 2x/a, \quad \eta = 2y/b \tag{2.9}$$

Because Kirchhoff's hypothesis was assumed, the plate is in an approximate state of plane stress. Using the plane stress constitutive equation for the kth layer, one has

$$\begin{Bmatrix} \sigma_x^{(k)} \\ \sigma_y^{(k)} \\ \sigma_{xy}^{(k)} \end{Bmatrix} = \begin{bmatrix} C_{11}^{(k)} & C_{12}^{(k)} & C_{13}^{(k)} \\ C_{12}^{(k)} & C_{22}^{(k)} & C_{23}^{(k)} \\ C_{13}^{(k)} & C_{23}^{(k)} & C_{33}^{(k)} \end{bmatrix} \begin{Bmatrix} \varepsilon_x \\ \varepsilon_y \\ \gamma_{xy} \end{Bmatrix} \tag{2.10}$$

where $C_{ij}^{(k)}$ are the reduced stiffnesses of the kth layer which can be obtained from E_L, E_T, major and minor Young's moduli , from the Poisson's ratios ν_{LT} and ν_{TL} and from the shear modulus G_{LT} [6]. L and T denote the principal directions of the orthotropic plate layer.

The stress resultants $\lfloor T_x \quad T_y \quad T_{xy} \rfloor$ and couples $\lfloor M_x \quad M_y \quad M_{xy} \rfloor$, all per unit length, are defined by

$$\lfloor T_x \quad T_y \quad T_{xy} \rfloor = \sum_{k=1}^{NL} \int_{z_{k-1}}^{z_k} \lfloor \sigma_x^{(k)}, \sigma_y^{(k)}, \sigma_{xy}^{(k)} \rfloor dz, \tag{2.11}$$

$$\lfloor M_x \quad M_y \quad M_{xy} \rfloor = \sum_{k=1}^{NL} \int_{z_{k-1}}^{z_k} \lfloor \sigma_x^{(k)} \sigma_y^{(k)} \sigma_{xy}^{(k)} \rfloor z \, dz. \tag{2.12}$$

where NL is the number of layers.

Combining (2.3) with (2.2), the strains can be expressed as

$$\varepsilon_x = u_{,x} + \frac{1}{2} w_{,x}^{\ 2} + z(-w_{,xx}) \tag{2.13a}$$

$$\varepsilon_y = v_{,y} + \frac{1}{2} w_{,y}^{\ 2} + z(-w_{,yy}) \tag{2.13b}$$

$$\gamma_{xy} = u_{,y} + v_{,x} + w_{,x} w_{,y} + z(-2w_{,xy}) \tag{2.13c}$$

or

$$\begin{Bmatrix} \varepsilon_x \\ \varepsilon_y \\ \gamma_{xy} \end{Bmatrix} = \begin{bmatrix} 1 & 0 & 0 & z & 0 & 0 \\ 0 & 1 & 0 & 0 & z & 0 \\ 0 & 0 & 1 & 0 & 0 & z \end{bmatrix} \{\varepsilon\} = [[I] \quad z[I]] \{\varepsilon\} \tag{2.13d}$$

where

$$\{\varepsilon\} = \begin{Bmatrix} \varepsilon_o^p \\ \varepsilon_o^b \end{Bmatrix} + \begin{Bmatrix} \varepsilon_L^p \\ 0 \end{Bmatrix} = \{\varepsilon_1\} + \{\varepsilon_2\} \tag{2.13e}$$

$$\{\varepsilon_o^p\} = \begin{Bmatrix} u_{,x} \\ v_{,y} \\ u_{,y} + v_{,x} \end{Bmatrix}, \quad \{\varepsilon_o^b\} = \begin{Bmatrix} -w_{,xx} \\ -w_{,yy} \\ -2w_{,xy} \end{Bmatrix}, \quad \{\varepsilon_L^p\} = \begin{Bmatrix} (w_{,x})^2/2 \\ (w_{,y})^2/2 \\ w_{,x} w_{,y} \end{Bmatrix} \tag{2.13f}$$

$\{\varepsilon_0^p\}$ and $\{\varepsilon_0^b\}$ are the linear membrane and bending strains and $\{\varepsilon_L^p\}$ is the geometrically nonlinear membrane strain.

Substituting equation (2.10) into equations (2.11) and (2.12) and using the relations (2.13), one arrives at the constitutive relations of the plate;

$$\begin{Bmatrix} T \\ M \end{Bmatrix} = \begin{bmatrix} A & B \\ B & D \end{bmatrix} \{\varepsilon\} = [E]\{\varepsilon\}, \tag{2.14}$$

with the membrane, coupling and flexural rigidities given by

$$\left(A_{ij}, B_{ij}, D_{ij}\right) = \sum_{k=1}^{NL} \int_{z_{k-1}}^{z_k} \left(1, z, z^2\right) C_{ij}^{(k)} \, \mathrm{d}z. \tag{2.15}$$

Because only isotropic and symmetric laminated plates will be analysed, there is no coupling between inplane stretching and transverse bending, therefore, $B_{ij} = 0$.

The equations of motion of the undamped plate are derived by equalising the sum of the virtual work of the inertia forces and of the elastic restoring forces, to the virtual work of the external forces. In this way one obtains

$$\begin{aligned} &\int_\Omega \left(\left\{\delta\varepsilon_o^p\right\}^T + \left\{\delta\varepsilon_L^p\right\}^T\right)[A]\left(\left\{\varepsilon_o^p\right\} + \left\{\varepsilon_L^p\right\}\right)\mathrm{d}\Omega \\ &\int_\Omega \left\{\delta\varepsilon_o^b\right\}^T [D]\left\{\varepsilon_o^b\right\}\mathrm{d}\Omega + \int_\Omega \rho h\left(\delta u_0 \ddot{u}_0 + \delta v_0 \ddot{v}_0 + \delta w_0 \ddot{w}_0\right)\mathrm{d}\Omega \\ &= \begin{bmatrix} \delta u_0 & \delta v_0 & \delta w_0 \end{bmatrix} \int_\Omega [N]^T \begin{Bmatrix} 0 \\ 0 \\ \overline{P}_d(x, y, t) \end{Bmatrix} \mathrm{d}\Omega, \end{aligned} \tag{2.16}$$

where ρ denotes the density, $\overline{P}_d(x, y, t)$ is the distributed force (N/m^2) applied perpendicularly to the plate and Ω is the area of the plate.

Substituting equation (2.13) into equation (2.16) and allowing the virtual generalised displacements to be arbitrary gives:

$$\begin{bmatrix} M_p & 0 \\ 0 & M_b \end{bmatrix}\begin{Bmatrix} \ddot{q}_p \\ \ddot{q}_w \end{Bmatrix}+\left(\begin{bmatrix} K1_p & 0 \\ 0 & K1_b \end{bmatrix}+\begin{bmatrix} 0 & K2 \\ 0 & 0 \end{bmatrix}+\begin{bmatrix} 0 & 0 \\ K3 & 0 \end{bmatrix}+\begin{bmatrix} 0 & 0 \\ 0 & K4 \end{bmatrix}\right)\begin{Bmatrix} q_p \\ q_w \end{Bmatrix}=\begin{Bmatrix} 0 \\ \overline{P} \end{Bmatrix} \tag{2.17}$$

where $[M_p]$ and $[M_b]$ are the in-plane and bending inertia matrices; $[K1_p]$ and $[K1_b]$ are the in-plane and bending linear stiffness matrices; $[K2]$, $[K3]$ and $[K4]$ are the nonlinear stiffness matrices and $\{\overline{P}\}$ is the vector of generalised external forces. A comprehensive derivation of these matrices by the HFEM is given by Han [11].

With the introduction of mass proportional hysteretic damping - which depends on the damping factors β_p and β - these equations become

$$\begin{bmatrix} M_p & 0 \\ 0 & M_b \end{bmatrix}\begin{Bmatrix} \ddot{q}_p \\ \ddot{q}_w \end{Bmatrix}+\begin{bmatrix} \frac{\beta_p}{\omega}M_p & 0 \\ 0 & \frac{\beta}{\omega}M_b \end{bmatrix}\begin{Bmatrix} \dot{q}_p \\ \dot{q}_w \end{Bmatrix}+\left(\begin{bmatrix} K1_p & 0 \\ 0 & K1_b \end{bmatrix}+\begin{bmatrix} 0 & K2 \\ K3 & K4 \end{bmatrix}\right)\begin{Bmatrix} q_p \\ q_w \end{Bmatrix}=\begin{Bmatrix} 0 \\ \overline{P} \end{Bmatrix} \tag{2.18}$$

All integrals involved in calculating the inertia and stiffness matrices in equation (2.18) were evaluated using symbolic computation [35]. All submatrices are symmetric except $[K2]$ and $[K3]$, which are related by $[K3]=2[K2]^T$.

Neglecting in-plane inertia and damping the following equations result from equation (2.18)

$$[M_b]\{\ddot{q}_w\}+\frac{\beta}{\omega}[M_b]\{\dot{q}_w\}+[K1_b]\{q_w\}+[Knl]\{q_w\}=\{\overline{P}\}, \tag{2.19}$$

where

$$[Knl]=[K4]-2[K2]^T[K1_p]^{-1}[K2]. \tag{2.20}$$

2.2 *Periodic motions and application of the Harmonic Balance Method*

In nonlinear vibrations, there are several parameters that influence the time dependence of the response: form of the external excitation, properties of the structure, initial and boundary conditions. Depending on these parameters, the oscillations may be periodic, including harmonic, sub-harmonic and super-harmonic motions; quasi-periodic or even chaotic [27]. A precise determination of the form of the response as a function of those parameters is, particularly in multiple degree of freedom systems, an interesting and complex field of research.

In this report only free vibration and vibration due to harmonic external excitations will be analysed. For various amplitudes and frequencies of excitation, time domain simulations of the response of the plates analysed were carried out. A one mode approach of equation (2.19) and a *Matlab* Runge-Kutta integration routine were used. For amplitudes of vibration of the order of the plates' thickness, the solution was always periodic and highly dominated by the harmonic with frequency equal to the excitation frequency or equal to the "nonlinear resonance frequency" in the free vibration case. Figures 2 and 3 show a typical result obtained.

Several time domain experimental analyses of the vibration of plates, with amplitudes of the order of the plates' thickness, resulted in periodic motion, dominated by the first harmonic [2, 4]. Moreover, in these references and in reference [51] it was experimentally verified that, as the amplitude of vibration displacement increases, there is a shape of vibration that, although changing smoothly, maintains a close resemblance to the linear mode shape.

The equations of motion (2.19) are of the Duffing type. The damped Duffing equation,

$$\ddot{w} + c\,\dot{w} + k\,w + knl\,w^3 = h(t) \qquad (2.21)$$

without forcing term, $h(t) = 0$, or with a forcing term $h(t)= h(t+T) \neq const$, real, continuous and periodic, in the hard spring case, $knl > 0$, and with non-negative damping, has a non-constant T-periodic solution (reference 9, pages 110 and 179).

Although other types of motion are possible, the experimental, numerical and analytical investigations just referred to confirm that periodic motion is the most likely to occur in plates vibrating with displacements of the order of their thickness, either freely or due to excitation by harmonic forces. The study of these periodic motions constitutes a relevant engineering and research problem, with still several difficulties to be overcome. These regard namely the study of higher order "modes", the reduction of the computational time needed to achieve accurate solutions and the implementation of methods capable of an automatic and complete description of the FRF curves of multi-degree-of-freedom systems.

There are two classic procedures that can be applied to obtain solutions of nonlinear differential equations: perturbation methods and the harmonic balance method (HBM). Perturbation methods, such as multiple scales and averaging [29] are restricted to weakly nonlinear systems. The HBM is not restricted to weakly nonlinear problems and has to its advantage the fact that for smooth systems the assumed periodic solutions always converge to the exact solution [16]. Another advantage of the HBM is its simplicity and easy computational implementation. The disadvantage of the HBM, when compared with perturbation methods, is that one must know which are the appropriate harmonics to use or to carry enough terms in the solution and check the order of the coefficients of all the neglected harmonics.

In this report the HBM will be applied and, in a first approximation, only one harmonic will be used. The use of more harmonics and subharmonics may lead to important conclusions, particularly with respect to super/subharmonic and internal resonances [18, 19, 21, 28]. It will be left for future work.

The excitations considered will be of the form: $\{\overline{P}\}= \{P\}\cos(\omega t)$. The steady state response $\{q_w(t)\}$ will be expressed as:

$$\{q_w(t)\}=\{w_c\}\cos(\omega t)+\{w_s\}\sin(\omega t) \tag{2.22}$$

This form of solution is inserted into the equations of motion (2.19) and the harmonic balance method (HBM) is applied. The equations of motion obtained are of the following form:

$$\{F\}=\left(-\omega^2\begin{bmatrix} M_b & 0 \\ 0 & M_b \end{bmatrix}+\begin{bmatrix} 0 & \beta M_b \\ -\beta M_b & 0 \end{bmatrix}+\begin{bmatrix} K1_b & 0 \\ 0 & K1_b \end{bmatrix}\right)\begin{Bmatrix} w_c \\ w_s \end{Bmatrix}+\begin{Bmatrix} F_1 \\ F_2 \end{Bmatrix}-\{P\}=\{0\}, \tag{2.23}$$

where

$$\{F_1\}=\frac{2}{T}\int_0^T[Knl]\{q_w\}\cos(\omega t)\mathrm{d}t=\left(\frac{3}{4}[KNL1]+\frac{1}{4}[KNL3]\right)\{w_c\}+\frac{1}{4}[KNL2]\{w_s\}, \tag{2.24}$$

$$\{F_2\}=\frac{2}{T}\int_0^T[Knl]\{q_w\}\sin(\omega t)\mathrm{d}t=\frac{1}{4}[KNL2]\{w_c\}+\left(\frac{1}{4}[KNL1]+\frac{3}{4}[KNL3]\right)\{w_s\}, \tag{2.25}$$

$$[KNL1]=\left[K4(\{w_c\},\{w_c\})\right]-2\left[K2(\{w_c\})\right]^T\left[K1_p\right]^{-1}\left[K2(\{w_c\})\right] \tag{2.26}$$

$$[KNL2]=\left[K4(\{w_c\},\{w_s\})\right]-2\left[K2(\{w_c\})\right]^T\left[K1_p\right]^{-1}\left[K2(\{w_s\})\right]^{1} -2\left[K2(\{w_s\})\right]^T\left[K1_p\right]^{-1}\left[K2(\{w_c\})\right] \tag{2.27}$$

[1] With this formulation, [*KNL*2] must be calculated using $2\left[N_{,x}^{w}\right]\{w_c\}\left[N_{,x}^{w}\right]\{w_s\}$.

$$[KNL3]=\left[K4\left(\{w_s\},\{w_s\}\right)\right]-2\left[K2\left(\{w_s\}\right)\right]^T\left[K1_p\right]^{-1}\left[K2\left(\{w_s\}\right)\right] \qquad (2.28)$$

$\left[K4\left(\{w_c\},\{w_c\}\right)\right]$ means quadratic function of $\{w_c\}$; $[KNL1]$, $[KNL2]$, $[KNL3]$, $[M_b]$ and $[K1_b]$ are symmetric. The vector of generalised displacements is defined by

$$\{w\}=\begin{Bmatrix} w_c \\ w_s \end{Bmatrix}. \qquad (2.29)$$

The total number of degrees of freedom of the model is $n=2p_o^2$, for a damped model, and $n=p_o^2$, for an undamped model.

3 THE CONTINUATION METHOD

To solve the system of equations (2.23), Newton's method is used in the nonresonant region. For each frequency, the first approximation of $\{w\}$ is the $\{w\}$ from last point of the FRF curve. By solving the following system of equations

$$[J]\{\delta w\} = -\{F\}, \tag{3.1}$$

$\{\delta w\}$ is obtained. $[J]$ is the Jacobian of $\{F\}$ defined by:

$$[J] = \partial\{F\}/\partial\{w\}. \tag{3.2}$$

A new approximation for $\{w\}$ is calculated by applying the following expression

$$\{w\} = \{w\}_{previous} + \delta\{w\}. \tag{3.3}$$

This procedure is repeated until convergence is achieved. The frequency is then changed to another fixed value and the same method applied.

In the vicinity of resonance frequencies there are multiple solutions, which are difficult to obtain with the Newton method alone. In these regions a continuation method, previously employed to study the vibration of beams [20, 36, 37], is utilised.

The continuation method is composed of two main loops. In the external loop a predictor to the solution is defined. For that, the two last determined points of the backbone curve - $(\{w\}_i, \omega_i^2)$ and $(\{w\}_{i-1}, \omega_{i-1}^2)$ - are used. The prediction of $\{w\}_{i+1}$ is thus obtained in the following way:

$$\{w\}_{i+1} = \{w\}_i + \Delta\{w\}_{i+1} \tag{3.4}$$

$$\Delta\{w\}_{i+1}=\left(\{w\}_i-\{w\}_{i-1}\right)\frac{dwaux}{wm} \tag{3.5}$$

dwaux is the amplitude of the first increment vector, $\Delta\{w\}_{i+1}$ and *wm* is the amplitude of the vector $\left(\{w\}_i-\{w\}_{i-1}\right)$. A prediction for ω_{i+1}^2 must also be calculated. This results from the equation

$$\omega_{i+1}^2=\omega_{i+1}^2+\Delta\omega_0^2 \tag{3.6}$$

$$\Delta\omega_0^2=\pm s/\left(\{\delta w\}_1^T\{\delta w\}_1\right)^{1/2} \tag{3.7}$$

s and $\{\delta w\}_1$ will be defined afterwards. The sign in equation (3.7) is chosen following that of the previous increment, unless the determinant of $[J]$ has changed sign. In the last case a sign reversal is applied. To calculate $\{\delta w\}_1$ in (3.7), the last known frequency of the FRF curve is used.

Now, the approximated solution must be corrected. This correction is carried out in an internal loop. Applying Newton method to equation (2.23) one arrives at:

$$[J]\{\delta w\}-[M]\ \{w\}_{i+1}\,\delta\omega^2=-\{F\}. \tag{3.8}$$

Note that, unlike equation (3.1), variations in the frequency are also considered. The fact that both the generalised displacements and the frequency are unknowns, allows one to pass the turning points of the backbone curve. However, there is one extra unknown: the frequency of vibration. Consequently, another equation is needed. This is obtained by constraining the

distance between the two successive points of the FRF curve, the arc-length s, to a fixed value by the following constraint equation

$$s^2 = \left\| \Delta\{w\}_{i+1} \right\|^2 \tag{3.9}$$

From equation (3.8), one has

$$\{\delta w\} = \delta\omega^2 \{\delta w\}_1 + \{\delta w\}_2 \tag{3.10}$$

$\{\delta w\}_1$ and $\{\delta w\}_2$ result from the equations

$$[J]\{\delta w\}_1 = [M]\ \{w\}_{i+1} \tag{3.11}$$

$$[J]\{\delta w\}_2 = -\ \{F\} \tag{3.12}$$

Note that $\{\delta w\}_1$ and $\{\delta w\}_2$ should be obtained by solving the systems of equations (3.11) and (3.12) and not by inversion of $[J]$, because the former leads to a smaller number of operations and to less numerical errors.

The corrected value of $\{w\}$ will be

$$\{w\}_{i+1} = \left(\{w\}_{i+1}\right)_{previous} + \Delta\{w\}_{i+1} \tag{3.13}$$

with

$$\Delta\{w\}_{i+1} = \left(\Delta\{w\}_{i+1}\right)_{previous} + \{\delta w\} \tag{3.14}$$

Substituting $\Delta\{w\}_{i+1}$ from equation (3.14) into the constraint equation (3.9) gives the relation for $\delta\omega^2$

$$a_1\left(\delta\omega^2\right)^2+a_2\,\delta\omega^2+a_3=0, \tag{3.15}$$

where

$$a_1=\{\delta w\}_1^T\{\delta w\}_1,\ a_2=2\left(\Delta\{w\}_i+\{\delta w\}_2\right)^T\{\delta w\}_1,$$
$$a_3=\left(\Delta\{w\}_i+\{\delta w\}_2\right)^T\left(\Delta\{w\}_i+\{\delta w\}_2\right)-s^2\ (31) \tag{3.16}$$

Equation (3.15) has two solutions. To avoid a return to the known part of the curve, the angle between the incremental amplitude vector of the previous iteration and the one of the present iteration should be positive. If both angles are positive the appropriate root is the one that is closer to the linear solution of equation (3.15).

The corrected value of the natural frequency is given by:

$$\Delta\omega^2{}_{i+1}=\Delta\omega^2{}_i+\delta\omega^2 \tag{3.17}$$

$$\omega^2{}_{i+1}=\omega_m^2+\Delta\omega^2{}_{i+1} \tag{3.18}$$

The iterations are repeated until the inequalities

$$\left|\left(\omega^2{}_{i+1}-\omega^2{}_i\right)/\omega^2{}_{i+1}\right|<error1 \tag{3.19}$$

$$\left\|\{w\}_{i+1}-\left(\{w\}_{i+1}\right)_{previous}\right\|/\left\|\{w\}_{i+1}\right\|<error2 \tag{3.20}$$

$$\left\|\{F\}\right\|<error3 \tag{3.21}$$

are satisfied. If the roots of equation (3.15) are complex, if too many iterations are necessary in order to achieve convergence or if $(\omega_{i+1} - \omega_i)$ is greater than the value desired by the user, then the arc-length is reduced and the process restarted from the previous know point of the backbone curve.

All the matrices necessary to obtain the FRF and backbone curves, including the Jacobian [*J*], were derived using the symbolic computation package *Maple* [35] and saved in files in *Fortran* format. The use of symbolic computation allows exact integration and differentation and, consequently, a very accurate determination of the matrices involved. The time spent in the formation of all the matrices was moderate due to the small number of DOF of the HFEM model. Both the Newton and continuation methods, which are iterative methods, were applied by means of a program written in *Fortran*. The solution of the equations of motion was speeded up because the matrices necessary to apply these methods are available in files.

4 STABILITY OF THE SOLUTIONS

To investigate the local stability of the harmonic solution a small disturbance is added to the steady state solution

$$\{\tilde{q}\}=\{q_w\}+\{\delta q_w\} \tag{4.1}$$

and its evolution is studied. If $\{\delta q_w\}$ dies out with time then $\{q_w\}$ is stable, if it grows then $\{q_w\}$ is unstable.

Inserting the disturbed solution (4.1) into equation (2.19), expanding the nonlinear terms by means of Taylor series around $\{q_w\}$ and ignoring terms of order higher than $\{\delta q_w\}$, the following equations are obtained:

$$[M_b]\{\delta\ddot{q}_w\}+\frac{\beta}{\omega}[M_b]\{\delta\dot{q}_w\}+[K1_b]\{\delta q_w\}+\frac{\partial([Knl]\{q_w\})}{\partial\{q_w\}}\{\delta q_w\}=\{0\}. \tag{4.2}$$

The coefficients $\partial([Knl]\{q_w\})/\partial\{q_w\}$ are periodic functions of time. With symbolic manipulation, they can easily be expanded in a Fourier series. If $\{q_w\}$ is of the form (2.22), then:

$$\frac{\partial([Knl]\{q_w\})}{\partial\{q_w\}}=[[p_1]+[p_2]\cos(2\omega t)+[p_3]\sin(2\omega t)], \tag{4.3}$$

$$[p_1]=\frac{1}{T}\int_0^T\frac{\partial}{\partial\{q_w\}}([Knl]\{q_w\})\,dt, \tag{4.4}$$

$$[p_2]=\frac{2}{T}\int_0^T\frac{\partial}{\partial\{q_w\}}([Knl]\{q_w\})\cos(2\omega t)dt, \tag{4.5}$$

$$[p_3]=\frac{2}{T}\int_0^T\frac{\partial}{\partial\{q_w\}}([Knl]\{q_w\})\sin(2\omega t)dt. \tag{4.6}$$

Multiplying equations (4.2) by the transpose of the modal matrix $[B]$ and using modal coordinates $\{\xi\}$, one arrives at:

$$\{\delta\ddot{\xi}\}+\frac{\beta}{\omega}[I]\{\delta\dot{\xi}\}+[\omega_j^2]\{\delta\xi\}+[B]^T([p_1]+[p_2]\cos(2\omega t)+[p_3]\sin(2\omega t))[B]\{\delta\xi\}=\{0\} \tag{4.7}$$

where $[\omega_j^2]$ is the diagonal matrix of linear natural frequencies.

This is a system of extended coupled Hill's equations. The first derivative term can be eliminated by introducing a new vector of variables

$$\{\delta\xi\}=e^{-\frac{1}{2}\frac{\beta}{\omega}[I]t}\{\delta\bar{\xi}\}, \tag{4.8}$$

obtaining, because matrix $e^{-\frac{1}{2}\frac{\beta}{\omega}[I]t}$ commutes with any other matrix and is non-singular,

$$\{\delta\ddot{\bar{\xi}}\}+\left([\omega_j^2]-\frac{1}{4}\left(\frac{\beta}{\omega}\right)^2[I]+[B]^T([p_1]+[p_2]cos(2\omega t)+[p_3]sin(2\omega t))[B]\right)\{\delta\bar{\xi}\}=\{0\} \tag{4.9}$$

where $[I]$ is the identity matrix.

Now, following Hayashi [17], the solution of (4.9) will be expressed in the form:

$$\{\delta\bar{\xi}\}=e^{\lambda t}\left(\{b_1\}\cos(\omega t)+\{a_1\}\sin(\omega t)\right) \tag{4.10}$$

which should allow one to determine, in a first approximation, the first order simple unstable region.

Inserting (4.10) into (4.9) and applying the HBM results in

$$\left(\lambda^2[I]+\lambda[M_1]+[M_0]\right)\begin{Bmatrix} b_1 \\ a_1 \end{Bmatrix}=\begin{Bmatrix} 0 \\ 0 \end{Bmatrix} \tag{4.11}$$

where

$$[M_1]=\begin{bmatrix} 0 & 2\omega[I] \\ -2\omega[I] & 0 \end{bmatrix} \tag{4.12}$$

$$[M_0]=\begin{bmatrix} [B]^T[J_{11}][B]-\left(\omega^2+\left(\frac{1}{2}\frac{\beta}{\omega}\right)^2\right)[I]+\left[{\omega_{0j}}^2\right] & [B]^T[J_{12}][B] \\ [B]^T[J_{21}][B] & [B]^T[J_{22}][B]-\left(\omega^2+\left(\frac{1}{2}\frac{\beta}{\omega}\right)^2\right)[I]+\left[{\omega_{0j}}^2\right] \end{bmatrix} \tag{4.13}$$

$$[J_{11}]=\frac{\partial\{F_1\}}{\partial\{w_c\}},\ [J_{12}]=\frac{\partial\{F_1\}}{\partial\{w_s\}},\ [J_{21}]=\frac{\partial\{F_2\}}{\partial\{w_c\}},\ [J_{22}]=\frac{\partial\{F_2\}}{\partial\{w_s\}}. \tag{4.14}$$

If no in-plane displacements are included in the model, the matrix $\partial([Knl]\{q_w\})/\partial\{q_w\}+[K1_b]$ is equivalent to the tangential stiffness matrix used in static analysis, $[K_T]$, which is symmetric [49, 50]. Since $[K1_b]$ is symmetric, $\partial([Knl]\{q_w\})/\partial\{q_w\}$ should also be symmetric. When the in-plane displacements are included and in-plane inertia neglected, it can be proved, by taking the appropriate variations, that $\partial([Knl]\{q_w\})/\partial\{q_w\}$ is still symmetric. This was aswell verified by inspection of the numerical values and of the expressions generated by a program written in *Maple*. Therefore, $[M_0]$ is a symmetric matrix.

To determine the characteristic exponents, λ, equations (4.11) are transformed into [46]

$$\begin{bmatrix} 0 & [I] \\ -[M_0] & -[M_1] \end{bmatrix} \begin{Bmatrix} X \\ \Gamma \end{Bmatrix} = \lambda \begin{Bmatrix} X \\ \Gamma \end{Bmatrix}, \tag{4.15}$$

where $\{X\}$ is a vector formed by $\{b_1\}$, $\{a_1\}$. The values of λ are the eigenvalues of the double size matrix in the previous equation. If the real part of $\lambda_r - \beta/(2\omega)$ is positive for any λ_r, then the solution is unstable, otherwise it is stable. Note that in order to study the solutions's stability just the major positive real part of λ_r must be calculated.

The determinant of the matrix [*J*] provides important information about the stability of the solutions, as is demonstrated in the following. The Floquet multipliers σ are related with the characteristis or Floquet exponents by

$$\sigma = e^{\left(\lambda_r - \frac{1}{2}\frac{\beta}{\omega}\right)t} \tag{4.16}$$

There are three ways in which stability can be lost [53]:

a) $\sigma=1 \Leftrightarrow \left(\lambda_r - \frac{1}{2}\frac{\beta}{\omega}\right)=0$

b) $\sigma=-1 \Leftrightarrow \left(\lambda_r - \frac{1}{2}\frac{\beta}{\omega}\right) = i\pi$

c) $\mathrm{Im}(\sigma) \neq 0 \Rightarrow \left(\lambda_r - \frac{1}{2}\frac{\beta}{\omega}\right)$ is a complex number

Mechanism *a*) of losing stability is characteristic of turning points and will be the only one considered in this report. Thus, the stability limit is defined by

$$\lambda = \frac{1}{2}\frac{\beta}{\omega}. \tag{4.17}$$

Inserting (4.17) in (4.11) one arrives at

$$\begin{bmatrix} [B]^T[J_{11}][B]-\omega^2[I]+[\omega_{0j}{}^2] & [B]^T[J_{12}][B]+\beta \\ [B]^T[J_{21}][B]-\beta & [B]^T[J_{22}][B]-\omega^2[I]+[\omega_{0j}{}^2] \end{bmatrix} \begin{Bmatrix} b_1 \\ a_1 \end{Bmatrix} = \begin{Bmatrix} 0 \\ 0 \end{Bmatrix} \tag{4.18}$$

The matrix in the previous equation is $[B]^T[J][B]$, where $[J]$ is the Jacobian of $\{F\}$ given by

$$[J]=\frac{\partial\{F\}}{\partial\{w\}} \tag{4.19}$$

A non-trivial solution of (4.18) exists if

$$\det\left([B]^T[J][B]\right)=0 \Leftrightarrow |B|^2|J|=0 \Leftrightarrow |J|=0, \tag{4.20}$$

The last equivalence is true because $[B]$ is a non-singular matrix, since the modal vectors are linearly independent; because the determinant of the product of matrices is equal to the product of the determinants and because the determinant of the tranpose matrix is equal to the determinant of the original matrix. Thus, it was proved that in the stability limit, the determinant of the Jacobian of $\{F\}$, $|J|$, is zero. This constitutes a generalization to mass proportionally damped systems of the demonstration presented in [20, 54 and 55] for undamped systems.

$|J|$ is a polynomial in $\{w_c\}$, $\{w_s\}$ and ω; therefore, it is a continuous function in those coefficients. All the experimental and numerical analysis of nonlinear vibration of plates, indicate that the shape of vibration, defined in this

model by $\{w_c\}$ and $\{w_s\}$, is a continuous function of the amplitude and the frequency of vibration. Thus, $|J|$ varies in a continuous way through the FRF curve. If there is a change in its sign between two consecutive points of the FRF curve, then $|J|=0$ for a particular point between these two. In that particular point, the stability limit might have been crossed.

So, a complete study of the first order solution's stability is carried out in the following way:

1 - determination of the stability of the first solution by finding the characteristic exponents. For low amplitudes of vibration, in the nonresonant area, this is not necessary. In fact, in these conditions the solution is always stable, as can be demonstrated by a perturbation method [45].

2 - calculation of $|J|$, which is needed in the continuation method and, when the Newton method is applied, can be easily calculated from $[J]$. If $|J|$ changes sign or if $|J|$ is approximatelly zero then calculate the characteristic exponents to verify if the stability of the solution changed.

It would seem evident, and all the numerical results indicate that if $|J|$ changes sign, then due to continuity $(\lambda - \beta/(2\omega))$ changes sign aswell; consequently a determination of the characteristic exponents does not appear to be necessary [20, 54, 55]. However, to be absolutely rigorous, one should remember that what was demonstrated was that $(\lambda - \beta/(2\omega))=0 \Rightarrow |J|=0$, nothing else.

5 APPLICATION TO ISOTROPIC PLATES

5.1 *Plates analysed*

The described methods were applied to two isotropic plates, Plates 1 and 2 - Table 1, with all edges immovable and clamped. Both plates are made of steel, with the properties: $E = 21.0\times10^{10}$ N/ m^2, $\nu = 0.3$, $\rho = 7800$ Kg/ m^3.

The external applied forces are harmonic plane waves at normal and grazing incidence.

5.2 *Convergence properties of the HFEM - free and forced vibration analysis*

Convergence studies for free and forced vibration were carried out using Plate 1. In this sub-section, the external excitation is a harmonic plane wave at normal incidence. Since the plate, the external excitation and the boundary conditions are symmetric with respect to both axes x and y, only modes for which the transverse displacement is symmetric with respect to x and y are excited. Thus, only symmetric out-of-plane shape functions need to be included in the model. However, both symmetric and antisymmetric in-plane shape functions must be used. This is so, because the in-plane displacements are anti-symmetric with respect to one axis but they are symmetric with respect to the other axis: $u(x,y)=u(x,-y)=-u(-x,y)$ and $v(x,y)=v(-x,y)=-v(x,-y)$.

When the excitation considered is a perpendicular harmonic plane wave, the force per unit area at an arbitrary point is given by $P_d \cos(\omega t)$, where P_d is the pressure amplitude. In this case the vector of generalised forces of equation (2.23) is

$$\{P\} = \begin{Bmatrix} \int_\Omega P_d \{N^w(x)\} d\Omega \\ 0 \end{Bmatrix} \tag{5.1}$$

The amplitude of the external applied pressure was 10 N/m^2. In all the figures in this section the amplitudes of vibration were calculated for $(x, y) = (0, 0)$.

The first four bi-symmetric linear modes of Plate 1 are shown in Figure 4. In Table 2, convergence of the linear natural frequencies with p_o is shown. In Figures 5, 6 and 7 the backbone curves and the frequency response function (FRF) curves are displayed for different values of p_o and for $p_i = 6$. Numerical values are given in Tables 3 - 5 for free vibration only. Because the parameter used in the continuation method is the arc-length, instead of the amplitude, the solutions are not obtained at exactly the same amplitudes. However, the numerical values shown give the reader an insight about the magnitude of the difference between results calculated with different number of shape functions. Results are only shown for the amplitudes attained in forced vibration. The solutions obtained with $p_o = 2$ are accurate around the first mode; for the second and third modes three out-of-plane shape functions provide a quite reasonable approximation to the solution.

In Figures 8, 9 and 10 the backbone curves and the FRF curves for forced vibration are displayed for different values of p_i, in all the cases $p_o = 3$. Tables 6-8 show the numeric values. It is concluded that, for the amplitudes considered, the results obtained with $p_i = 4$ are quite accurate. It is also shown that the exclusion of the in-plane displacements ($p_i = 0$) increases the stiffness of the model. The influence of the in-plane displacements is particularly visible around the first mode, probably due to the larger amplitudes of vibration attained at the point (0, 0) with this mode.

5.3 *Comparison with experimental and theoretical results*

In order to validate the model, the results using $p_o = 3$ and $p_i = 6$ were compared with experimental and other theoretical results.

For Plate 2, comparison is made in Tables 9 between the HFEM free and forced vibration results and results from the literature. The agreement with Han and Petyt's [14] free vibration results is excellent. Because use was made here of the symmetry properties of the structure, far fewer degrees of freedom were used then in reference [14]. In Table 10, comparison is made with forced vibration results. The values of low amplitude forced vibration, are not so close to published ones as values of vibration at higher amplitudes. This is strange since at low amplitudes, we are nearer the linear zone, for which the method used should not be so important. The difference may be explained by some small inaccuracy in the calculation of the actual applied pressure amplitude from the nondimensional values given in [24]. Since the small amplitudes occur far way from the resonance area, a small deviation in the applied force implies a visible deviation in the amplitude attained. In Figure 11 the first resonance frequencies obtained with the HFEM, for Plate 1, are compared with the experimental ones. With the exception of a curious deviation in the last experimentally obtained point, the HFEM and continuation methods results agree well with the experimental ones.

5.4 *Study of Stability*

The method described in section 4 was applied to study the stability of the solutions. The results obtained are shown in Figures 12-14.

5.5 *Response to a harmonic plane wave at grazing incidence*

When the excitation considered is a grazing acoustic harmonic plane wave, the force per unit area at an arbitrary point is given by $P_g \cos(\omega t - kx)$, with $k = \frac{\omega}{c}$ and where P_g is the pressure amplitude, k is the wave number and c is the speed of sound in air. In this case the vector of generalised forces of equation (2.18) is

$$\{P\} = \begin{Bmatrix} \int_\Omega P_g \cos\left(k(x\cos\alpha + y\sin\alpha)\right)\{N^w\}d\Omega \\ \int_\Omega P_g \sin\left(k(x\cos\alpha + y\sin\alpha)\right)\{N^w\}d\Omega \end{Bmatrix} =$$

$$\begin{Bmatrix} \frac{P_g ab}{4}\int_{-1}^{1}\int_{-1}^{1}\cos\left(\frac{ka\xi}{2}\cos\alpha + \frac{kb\eta}{2}\sin\alpha\right)\{N^w\}d\eta d\xi \\ \frac{P_g ab}{4}\int_{-1}^{1}\int_{-1}^{1}\sin\left(\frac{ka\xi}{2}\cos\alpha + \frac{kb\eta}{2}\sin\alpha\right)\{N^w\}d\eta d\xi \end{Bmatrix} \qquad (5.2)$$

where α is the angle between the direction of propagation of the wave and the positive x axis. The last expression is simplified to

$$\{P\} = \begin{Bmatrix} \int_\Omega P_g \cos(kx)\{N^w\}d\Omega \\ \int_\Omega P_g \sin(kx)\{N^w\}d\Omega \end{Bmatrix} = \begin{Bmatrix} \frac{P_g ab}{4}\int_{-1}^{1}\int_{-1}^{1}\cos\left(\frac{ka\xi}{2}\right)\{N^w\}d\eta d\xi \\ \frac{P_g ab}{4}\int_{-1}^{1}\int_{-1}^{1}\sin\left(\frac{ka\xi}{2}\right)\{N^w\}d\eta d\xi \end{Bmatrix} \qquad (5.3)$$

if the wave is travelling in the direction of the x axis of the plate (α=0).

The quite complex expressions for the vector of generalised forces were generated using Maple. They were very affected by numerical round-off errors; therefore it was necessary to use a large number of digits to derive them.

A wave at grazing incidence, travelling along the longitudinal axis of the plate, excites only modes that are symmetric in y, but excites both symmetric

and anti-symmetric modes in x. In Figures 15, 16 and 17 the FRFs in the vicinity of the first, second and third modes, obtained when an excitation at P_g of 10 N/m^2 was applied are shown. Since only four (two symmetric and two anti-symmetric) out of plane shape functions were used, the results around the third mode (second symmetric mode) should be interpreted in a qualitative way.

6 APPLICATION TO LAMINATED PLATES

6.1 *Plates analysed*

For simplicity only laminated plates which are symmetric about their middle plane, and consequently, for which there is no coupling between transverse bending and in-plane stretching, $[B]=[0]$, are investigated. The properties of the laminated plates analysed are shown in Tables 11a and 11b.

Both symmetric and antisymmetric out and in-plane shape functions must be used because the modes of vibration of laminated plates are asymmetric.

The loss factor generally assumes a value between 0.01 and 0.1, for the common type of composite panel used in aircraft construction [25]. In this report 0.01 will be utilised.

6.2 *Plate 3*

The first four linear modes of vibration of Plate 3 are shown in Figure 18.

In the following sections, convergence studies are carried out for free and forced vibration and the results are compared with published results.

6.2.1 *Influence of out-of-plane displacements in free and forced vibration*

The convergence of the linear natural frequencies is shown in Table 12. The relative error between the third linear frequency obtained with p_o=4 and p_o=6 is only 2.4%.

Although the plate is not symmetric about the planes defined by axes x-z and by axes y-z, a normal applied wave does not excite visibly the second and third modes. Consequently convergence in forced vibration was only studied for the first mode. In Figures 19 and 20 the convergence with p_o for free and forced vibration of mode 1 and free vibration of modes two and three is shown. For the first three modes of vibration, and for the amplitudes considered, p_o = 4 provides quite accurate results.

6.2.2 *Influence of in-plane displacements in free and forced vibration*

In Figures 21 and 22 the convergence with p_i for free and forced vibration of mode 1 and free vibration of modes two and three is shown. For the first three modes of vibration, and for the amplitudes considered, p_i = 6 provides accurate results. Four in-plane shape functions are enough for the first mode of vibration. Note that if not enough shape functions are used, the model becomes more stiff. This is particularly true for larger amplitudes of vibration displacement.

6.2.3 *Comparison with published results*

In Tables 12-14, the results obtained with the HFEM and continuation method are compared with published ones.

Note in Table 12, that with p_o=3 (9 DOF), the fundamental linear frequency value is below, and closer to the accurate one, the value obtained

with 36 elements and 24 DOF per element in reference [8] (to make a fair comparison, we should note that 8 of this 24 DOF, the inplane nodal displacements, would not be necessary in linear analysis).

The value of the natural frequency obtained when the plate vibrates with a maximum amplitude equal to its thickness is very close to the one given in [15], obtained with the HFEM and an iterative method - Table 13.

The values from forced vibration are close to the ones presented in reference [8] - Table 14. Note that more in-plane then out-of-plane shape functions are needed for convergence.

6.3 *Plate 4*

After the experience with isotropic plates and with Plate 3, it is expected that the number of shape functions necessary for convergence in forced vibration, will be the same as in free vibration, thus convergence studies will be only carried out for free vibration. As with Plate 3, both symmetric and antisymmetric out and in-plane shape functions must be used because the modes of vibration of laminated plates are asymmetric (with the exception of cross-ply plates).

The first four modes of vibration of Plate 4 are shown in Figure 23.

6.3.1 *Influence of out-of-plane displacements. Free vibration analysis*

The convergence of the linear natural frequencies is shown in Table 15. The relative error between the third natural frequency value obtained with p_o=3 and p_o=7 is 2.4%. In Tables 16 - 18 the values of the nondimensional frequency of vibration, in function of the nondimensional amplitude of vibration, are displayed for different values of p_o. For the first three modes of vibration, and

for the amplitudes considered, p_o = 4 or even p_o=3, provide quite accurate results. Note that the variation of ω/ω_1 with amplitude is similar with p_o= 3, 4 or 5. The error due to using less out-of-plane shape functions is not much higher in nonlinear than in linear analysis.

6.3.2 *Influence of in-plane displacements. Free vibration analysis.*

In Tables 19 - 21 one can see the convergence with the number of in-plane shape functions. It is concluded that, for the amplitudes considered, p_i = 4 are enough for the first mode, but more in-plane shape functions are necessary for higher order modes.

6.3.3 *Comparison with published results in free vibration analysis*

In order to validate the model and the methods of solution, in Table 22 the results obtained with the HFEM and with the continuation method are compared with results obtained with the HFEM and an iterative method [15]. The agreement is excellent.

6.3.4 *Steady-state forced vibration analysis*

In Figures 24-33 FRF curves due to harmonic plane waves and plane waves at grazing incidence are displayed. The method based on the sign of $|J|$, presented in section 4, was applied to study the stability of the solutions. In order to confirm this results a full determination of the characteristic exponents was carried out.

7 CONCLUSIONS

Free and steady-state forced vibration of isotropic and laminated plates modelled by the HFEM were analysed. With a small number of DOF the FRF and backbone curves were determined up to the 3rd order mode. By comparison with experimental and numerical results, the model was validated.

Employing the flexibility of choosing different shape functions to construct the HFEM model, it was demonstrated that the use of less in-plane shape functions than necessary increases the stiffness of the model. The influence of in-plane shape functions increases with the increase of the amplitude of vibration. On the other hand, for the cases studied, it was observed that the number of out-of-plane displacement shape functions necessary to obtain convergence in nonlinear analysis is roughly the same as in linear analysis. For large amplitudes of vibration, more in-plane than out-of-plane shape functions are necessary in order to achieve convergence. This is explained by the facts that for each out-of-plane wave, there are two in-plane waves, and that larger amplitudes of vibration displacement imply larger non-linearity.

With the continuation method the FRF and backbone curves were completely and automatically described. Unlike other methods, in which convergence is not achieved because the generalised displacements "jump" between different modes of vibration in successive iterations [11], this method found no problem in achieving convergence in frequency regions where more then one mode exist. This proves the numerical capability of the method. However, it does not exclude the hypothesis of interaction between different modes, due to internal resonance. This interaction may be studied by including more terms in the Fourier time series.

The applied continuation method is quite powerful, mainly because of its ability to pass turning and bifurcation[3] points, thus describing multi-valued

[3] To find an application of the same continuation method to a case with bifurcation points see reference [36].

regions. However, this method is computationally heavier than other iterative methods applied in nonlinear analysis. The advantage of using the HFEM to model the structure with a small number of degrees of freedom is consequently enhanced. This is the first application, known to the authors, of this continuation method to free and forced nonlinear vibration of either isotropic or laminated plates, as well as the first application of the HFEM to the analysis of nonlinear forced vibration of plates.

For mass proportionally damped systems it was proved that the determinant of the Jacobian of $\{F\}$, $|J|$, is zero in the stability limit. Thus, one only has to determine the characteristic exponents of the first solution and after an indication that $|J|$ was zero. The eigenvalue problem which defines the characteristic exponents, was quickly solved due to the reduced number of degrees of freedom of the HFEM model.

ACKNOWLEDGEMENT

P. Ribeiro acknowledges the support of PRAXIS XXI, *JNICT*, Portugal.

REFERENCES

[1] - Bardell, N. S. 1991. Free vibration analysis of a flat plate using the hierarchical finite element method. *J. of Sound and Vibr.* 151(2): 263-289.

[2] - Benamar, R 1990. *Nonlinear dynamic behaviour of fully clamped beams and rectangular isotropic and laminated plates.* Ph.D. Thesis. University of Southampton. UK.

[3] - Benamar, R., Bennouna, M.M.K. & White, R. G. 1993. The effects of large vibration amplitudes on the mode shapes and natural frequencies of thin elastic structures, part II: fully clamped rectangular isotropic plates. *J. of Sound and Vibr.* 164(2): 295-316.

[4] - Benamar, R., Bennouna, M.M.K. & White, R. G. 1994. The effects of large vibration amplitudes on the mode shapes and natural frequencies of thin elastic structures, part III: fully clamped rectangular isotropic plates-measurements of the mode shape amplitude dependence and the spatial distribution of harmonic distortion. *J. of Sound and Vibr.* 175(3): 377-395.

[5] - Berger, H. M. 1955. A new approach to the analysis of large deflections of plates. *Trans. ASME, J. Appl. Mech.* 22: 456-472.

[6] - Chia, C.Y. 1980. *Nonlinear Analysis of Plates.* United States of America: MacGraw-Hill.

[7] - Chia, C.Y. 1988. Geometrically nonlinear behavior of composite plates: a review. *Appl. Mech. Rev.* 41(12): 439-451.

[8] - Chiang, C. K., Mei, C. & Gray, C. E. 1991. Finite element large-amplitude free and forced vibrations of rectangular thin composite plates. *Trans ASME, J. Vibr. Acoustics* 113: 309-315.

[9] - Farkas, M. 1994. *Periodic Motions.* New York: Springer-Verlag.

[10] - Ganapathi, M; Varadan, T. K. & Sarma, B. S. 1991. Nonlinear flexural vibrations of laminated orthotropic plates. *Computers & Structures* 39(6): 685-688.

[11] - Han, W. 1993. *The Analysis of isotropic and laminated rectangular plates including geometrical non-linearity using the p-version finite element method.* Ph.D. Thesis. University of Southampton. UK.

[12] - Han, W. & Petyt, M. 1996. Linear vibration analysis of laminated rectangular plates using the hierarchical finite element method - I: Free vibration analysis. *Computers and Struct.* 61 (4): 705-712.

[13] - Han, W. & Petyt, M. 1996. Linear vibration analysis of laminated rectangular plates using the hierarchical finite element method - II: Forced vibration analysis. *Computers and Struct.* 61 (4): 713-724.

[14] - Han, W. & Petyt, M. 1997. Geometrically nonlinear vibration analysis of thin, rectangular plates using the hierarchical finite element method - I: The fundamental mode of isotropic plates. *Computers and Struct.* 63 (2): 295-308.

[15] - Han, W. & Petyt, M. 1997. Geometrically nonlinear vibration analysis of thin, rectangular plates using the hierarchical finite element method - II: 1st mode of laminated plates and higher modes of isotropic and laminated plates. *Computers and Struct.* 63 (2): 309-318.

[16] - Hamdan, M.N. & Burton, T.D. 1993. On the steady state response and stability of non-linear oscillators using harmonic balance. *J. of Sound and Vibr.* 166: 255-266.

[17] - Hayashi, C. 1964. *Nonlinear Oscillations in Physical Systems.* New York: McGraw-Hill.

[18] - Lau, S. L.; Cheung, Y. K. & Wu, S. Y. 1984. Nonlinear vibration of thin elastic plates. Part 1: Generalised incremental Hamilton's principle and element formulation. *Trans. ASME, J. Appl. Mech.* 51: 837-844.

[19] - Lau, S. L.; Cheung, Y. K. & Wu, S. Y. 1984. Nonlinear vibration of thin elastic plates. Part 2: Internal resonance by amplitude-incremental finite element. *Trans. ASME, J. Appl. Mech.* 51: 845-851.

[20] - Lewandowski, R. 1991. Non-linear, steady-state analysis of multispan beams by the finite element method. *Computers and Struct.* 39(1,2): 83-93.

[21] - Lewandowski, R. 1996. On beams membranes and plates vibration backbone curves in cases of internal resonance. *Meccanica.* 31: 323-346.

[22] - Maestrello, L.; Frendi, A. & Brown, D.E. 1992. Nonlinear vibration and radiation from a panel with transition to chaos. *AIAA Journal.* 30 (11): 2632-2638.

[23] - Mei, C. 1973. Finite element displacement method for large amplitude free flexural vibration of beams and plates. *Computers and Struct* 3: 163-174.

[24] - Mei, C. & Decha-Umphai, K 1985. A finite element method for non-linear forced vibrations of rectangular plates. *AIAA Journal.* 23(7): 1104-1110.

[25] - Mei, C. & Prasad, C.B. 1989. Effects of large deflection and transverse shear on responses of symmetrical composite laminates subjected to acoustic excitation. *J. Comp. Materials* 23(6): 606-639.

[26] - Meirovitch, L. 1986. *Elements of Vibration Analysis.* Singapore: McGraw-Hill.

[27] - Moon, F. C. 1987. *Chaotic Vibrations. An Introduction for Applied Scientists and Engineers.* New York: John Wiley & Sons.

[28] - Nayfeh, A H & Balachandran 1989. Modal interactions in dynamical and structural systems. *Appl. Mech. Rev.* 42(11 - Part 2): S175 - S201.

[29] - Nayfeh & Mook, 1995. *Nonlinear Oscillations.* New York: John Wiley & Sons.

[30] - Prabhakara, M. K. & Chia, C. Y. 1977. Non-linear flexural vibrations of orthotropic plates. *Journal of Sound and Vibration* 52(4): 511-518.

[31] - Prathap, B. S. & Varadan, T. K. 1978. The large amplitude vibrations of hinged beams. *Comput. and Struct.* 9: 219-222.

[32] - Rao, G. V.; Raju, I. S. & Raju, K. K. 1976. A finite element formulation for large amplitude flexural vibrations of thin rectangular plates. *Comput. Struct.* 6: 163-167.

[33] - Rao, S. & Mukhopadhyay, M. 1993. Large-amplitude finite element flexural vibration of plates/stiffened plates. *J. Acoust. Soc. Am.* 93(6): 3250-3257.

[34] - Reddy, J. N. & Chao, W. C. 1981. Large-deflection and large-amplitude free vibrations of laminated composite-material plates. *Comput. Struct.* 13: 341-347.

[35] - Redfern, D. 1994. *The Maple Handbook.* New York: Springer-Verlag.

[36] - Ribeiro, P. & Petyt, M. 1995. *Study of nonlinear free vibration of beams by the hierarchical finite element method.* ISVR Technical Memorandum No. 773.

[37] - Ribeiro, P. & Petyt, M. 1997. *Nonlinear forced vibration of beams by the hierarchical finite element and continuation methods.* ISVR Technical Memorandum No. 814.

[38] - Sarma, M. S.; Rao A. V.; Pillai, S. R. R. & Rao, B. N. 1992. Large amplitude vibrations of laminated hybrid composite plates. *J. Sound Vibr.* 159: 540-545.

[39] - Sarma, M. S. & Rao, B. N. 1995. Applicability of the energy method to non-linear vibrations of thin rectangular plates. *J. Sound Vibr.* 159: 540-545.

[40] - Sathyamoorthy, M. 1978. Nonlinear vibration of rectangular plates. *J. Sound Vibr.* 58(2): 301-304.

[41] - Sathyamoorthy, M. 1987. Nonlinear vibration analysis of plates: a review and survey of current developments. *Appl. Mech. Rev.* 40(11): 1553-1561.

[42] - Schwartz, M. M. 1992. *Composite materials handbook.* Second Edition. New York: McGraw-Hill, Inc.

[43] - Singh, G.; Raju, K. K.; Rao, G. V. & Iyengar, N.G.R. 1990. Non-linear vibrations of simply supported rectangular cross-ply plates. *J. Sound Vibr.* 142(2): 213-226.

[44] - Smith, P. W.; Malme, C. I. & Gogos, C. M. 1961. Nonlinear response of a simple clamped panel. *The J. of the Acoust. Soc. of America.* 33(11): 1476-1482.

[45] - Szemplinska-Stupnicka, W. 1990. *The Behaviour of Non-linear Vibrating Systems.* Dordretch: Kluwer Academic Publishers.

[46] - Takahashi, K. 1979. A method of stability analysis for non-linear vibration of beams. *J. of Sound and Vibr.* 67(1): 43-54.

[47] - Teh, C. E. 1982. *Dynamic behaviour and acoustic fatigue of isotropic and anisotropic panels under combined acoustic excitation and static in-plane compression.* Ph.D. Thesis. University of Southampton. UK.

[48] - Tseng, W. Y. & Dugundji, J. 1970. Nonlinear vibrations of a beam under harmonic excitation. *Transactions of the ASME, Journal of Applied Mechanics.* 37: 292-297.

[49] - Zienkiewicz, O.C. & Taylor, R.L. 1988. *The Finite Element Method.* 4th Edition. London: McGraw-Hill.

[50] - Waszczyszyn, Z; Cichon, C & Radwanska, M 1994. *Stability of Structures by Finite Element Methods.* Amsterdam: Elsevier Science B.V.

[51] - Wolfe, H. 1995. *An experimental investigation of nonlinear behaviour of beams and plates excited to high levels of dynamic response*; Ph.D. Thesis, University of Southampton.

[52] - Woo, J. & Nair, S. 1992. Nonlinear vibrations of rectangular laminated thin plates. *AIAA Journal* 30(1): 180-188.

[53] - Seidel, R. 1988. *From equilibrium to chaos. Pratical bifurcation and stability analysis.* New York: Elsevier Science Publishing Co., Inc.

[54] - Lewandowski, R. 1997. Computational formulation for periodic vibration of geometrically nonlinear structures - Part 1: Theoretical background. *Int. J. Solids Structures* 34(15): 1925-1947.

[55] - Lewandowski, R. 1997. Computational formulation for periodic vibration of geometrically nonlinear structures - Part 2: Numerical strategy and examples. *Int. J. Solids Structures* 34(15): 1949-1964.

TABLES

Table 1 - Geometric properties of Plates 1 and 2

Plate	a (mm)	b (mm)	h (mm)
1	486	322.9	1.2
2	500	500	2.0833

Table 2 - Convergence of linear natural frequencies of Plate 1 with p_o. Bi-symmetric modes.

p_o	2	3	4	5
ω_1 (rad/s)	487.343	487.283	487.276	487.276
ω_2 (rad/s)	1233.04	1197.30	1195.92	1195.91
ω_3 (rad/s)	2378.31	2267.64	2263.73	2263.69

Table 3 - Convergence of frequency ratios ω/ω_1 of the fundamental mode with p_o. Plate 1. p_i=6.

p_o=2		p_o=3		p_o=4		p_o=5	
$\frac{w_{max}}{h}$	ω/ω_1	$\frac{w_{max}}{h}$	ω/ω_1	$\frac{w_{max}}{h}$	ω/ω_1	$\frac{w_{max}}{h}$	ω/ω_1
0.20112	1.0075	0.19308	1.0069	0.25820	1.0123	0.19935	1.0073
0.39781	1.0290	0.40502	1.0299	0.41981	1.0321	0.39991	1.0291
0.59444	1.0637	0.59830	1.0644	0.60211	1.0653	0.59950	1.0644
0.79931	1.1129	0.79760	1.1124	0.79957	1.1131	0.79906	1.1121
1.0004	1.1730	1.0003	1.1729	1.0265	1.1817	1.0000	1.1711

Table 4 - Convergence of the frequency ratios ω/ω_1 of the second mode with p_o. Plate 1. p_i=6.

p_o=2		p_o=3		p_o=4		p_o=5	
$\frac{w_{max}}{h}$	ω/ω_1			$\frac{w_{max}}{h}$	ω/ω_1	$\frac{w_{max}}{h}$	ω/ω_1
0.22911	2.6121	0.22982	2.5369	0.22991	2.5324	0.23046	2.5325

Table 5 - Convergence of the frequency ratios ω/ω_1 of the third mode with p_o. Plate 1. p_i=6.

p_o=2		p_o=3		p_o=4		p_o=5	
$\frac{w_{max}}{h}$	ω/ω_1	$\frac{w_{max}}{h}$	ω/ω_1	$\frac{w_{max}}{h}$	ω/ω_1	$\frac{w_{max}}{h}$	ω/ω_1
0.25094	5.1332	0.25010	4.8929	0.24903	4.8770	0.24971	4.8761

Table 6 - Convergence of frequency ratios ω/ω_1 of the fundamental mode with p_i. Plate 1. p_o=3.

p_i=0		p_i=2		p_i=3		p_i=4	
$\frac{w_{max}}{h}$	ω/ω_1	$\frac{w_{max}}{h}$	ω/ω_1	$\frac{w_{max}}{h}$	ω/ω_1	$\frac{w_{max}}{h}$	ω/ω_1
0.19725	1.0105	0.20767	1.0116	0.20553	1.0107	0.20124	1.0080
0.41032	1.0443	0.39996	1.0421	0.39880	1.0398	0.39927	1.0309
0.59209	1.0899	0.60250	1.0928	0.59809	1.0872	0.59901	1.0682
0.79722	1.1566	0.79983	1.1574	0.80076	1.1509	0.80063	1.1188
1.0025	1.2363	0.99991	1.2353	1.0002	1.2261	0.99971	1.1799

p_i=5		p_i=6	
$\frac{w_{max}}{h}$	ω/ω_1	$\frac{w_{max}}{h}$	ω/ω_1
0.20369	1.0081	0.19308	1.0069
0.40135	1.0309	0.40502	1.0299
0.59977	1.0679	0.59830	1.0644
0.79990	1.1179	0.79760	1.1124
1.0003	1.1792	1.0003	1.1729

Table 7 - Convergence of frequency ratios ω/ω_1 of the second mode with p_i. Plate 1. p_o=3.

HFEM p_i=0		HFEM p_i=2		HFEM p_i=3		HFEM p_i=4		HFEM p_i=5	
$\frac{w_{max}}{h}$	ω/ω_1	$\frac{w_{max}}{h}$	ω/ω_1	$\frac{w_{max}}{h}$	ω/ω_1	$\frac{w_{max}}{h}$	ω/ω_1	$\frac{w_{max}}{h}$	ω/ω_1
0.25000	2.5553	0.24996	2.5523	0.25004	2.5523	0.24993	2.5517	0.24990	2.5515

Table 8 - Convergence of the frequency ratios ω/ω_1 of the third mode with p_i. Plate 1. p_o=3.

p_i=0		p_i=2		p_i=3		p_i=4	
$\frac{w_{max}}{h}$	ω/ω_1	$\frac{w_{max}}{h}$	ω/ω_1	$\frac{w_{max}}{h}$	ω/ω_1	$\frac{w_{max}}{h}$	ω/ω_1
0.25011	4.9037	0.25001	4.8941	0.24993	4.8934	0.25007	4.8936

p_i=5		p_i=6	
$\frac{w_{max}}{h}$	ω/ω_1	$\frac{w_{max}}{h}$	ω/ω_1
0.24994	4.8932	0.25010	4.8929

Table 9 - Comparison of frequency ratios ω/ω_1 of immovable fully clamped square isotropic plates.

$\frac{w_{max}}{h}$	Han & Petyt [14] p_o=p_i=7	Rao et al [33]	HFEM p_o=3 p_i=6		HFEM p_o=4 p_i=7	
			$\frac{w_{max}}{h}$	ω/ω_1	$\frac{w_{max}}{h}$	ω/ω_1
0.2	1.0068	1.0095	0.2099	1.0079	0.21377	1.0082
0.6	1.0600	1.0825	0.6007	1.0632	0.60780	1.0647
1	1.1599	1.2149	1.0011	1.1670	1.0012	1.1668

Table 10 - Frequency ratio ω/ω_1 of immovable fully clamped isotropic square plates under uniform harmonic distributed force P_0=0.2* (P_d=873.82 N/m^2).

$\frac{w_{max}}{h}$	Elliptic function solution*	Perturbation solution*	Finite element*	HFEM p_o=3 p_i=6		HFEM p_o=4 p_i=7	
				$\frac{w_{max}}{h}$	ω/ω_1	$\frac{w_{max}}{h}$	ω/ω_1
±0.2	0.1944	0.1987	0.1643	+.2001	0.2442	+0.2000	0.2432
	1.4281	1.4281	1.4238	-.2005	1.4399	-0.2072	1.4275
±0.6	0.8951	0.8956	0.8905	+.5992	0.8962	+0.6008	0.8971
	1.2117	1.2119	1.2083	-.5997	1.2114	-0.59011	1.2120
±1	1.0822	1.0845	1.0700	+1.000	1.0800	1.0013	1.0803
	1.2540	1.255	1.2429	-1.001	1.2491	-0.9952	1.2475

* From reference [24]: $P_0 = cF_0/\rho h^2\omega_1^2$ $c = \iint \phi dxdy / \iint \phi^2 dxdy$, ϕ - normalised mode shape. F_0 - amplitude of external applied force (N/m^2).

Table 11a - Geometric properties of laminated plates

Plate	Number of layers	Orientation of principal axes	a (mm)	b (mm)	h (mm)
3	3	(45, -45, 45)	500	500	5
4	8	$(90, -45, 45\ 0)_{sym.}$	480	320	1

Table 11b - Material properties of laminated plates

Plate	E_L(GNm^{-2})	E_G(GNm^{-2})	G_{LT}(GNm^{-2})	ν_{LT}
3	206.84	5.171	2.5855	0.25
4	120.5	9.63	3.58	0.32

Table 12 - Convergence of linear natural frequencies of Plate 3 with number of out-of-plane shape functions.

p_o	3	4	5	6	ref [8]
ω_1 (rad/s)	1587.01	1580.36	1576.72	1574.96	1592.30
ω_2 (rad/s)	2688.01	2580.91	2578.71	2577.55	—
ω_3 (rad/s)	4041.70	3759.85	3690.61	3671.02	—

Table13 - Free vibration. Plate 3. Comparison with reference [15] results. $\xi=\eta=0$.

$\frac{w_{max}}{h}$	Han & Petyt [15] $p_o=p_i=5$ ω/ω_1	HFEM and Continuation Met. $p_o=p_i=5$ $\frac{w_{max}}{h}$	ω/ω_1
1	1.2268	0.99897	1.2259

Table 14 - Forced vibration. Plate 3. Comparison with reference [8] results. P_0=0.1* (P_d = 3454.6650 N/m^2). ξ=η=0.

HFEM p_o=4		HFEM p_o=4		HFEM p_o=5		reference [8]	
$\frac{w_{max}}{h}$	p_i=6 ω/ω_1	$\frac{w_{max}}{h}$	p_i=7 ω/ω_1	$\frac{w_{max}}{h}$	p_i=5 ω/ω_1	$\frac{w_{max}}{h}$	ω/ω_1
0.20163	0.73401	0.20184	0.73401	0.20117	0.73570	±0.2	0.7219
-0.19709	1.24655	-0.20000	1.24321	-0.19981	1.24520		1.2333
0.39441	0.91119	0.39631	0.91119	0.40336	0.91963	±0.4	0.9129
-0.39993	1.15836	-0.40036	1.15726	-0.39407	1.16099		1.1548
0.59965	1.00845	0.60001	1.00687	0.60199	1.01498	±0.6	1.0085
- 0.60001	1.16395	-0.59972	1.16225	-0.60311	1.16824		1.1621
0.800173	1.091817	0.799681	1.08950	0.79874	1.09893	±0.8	1.0929
-0.79988	1.201822	-0.80035	1.19995	-0.80208	1.20842		1.2018
1.00053	1.17560	0.99984	1.17312	1.00172	1.18607	±1	1.1787
-0.99987	1.25782	-0.99993	1.25580	-0.99818	1.26571		1.2607

* From reference [8]. $P_0 = cF_0/\rho h^2\omega_1^2$ $c = \iint \phi dxdy / \iint \phi^2 dxdy$, ϕ - normalised mode shape. F_0 - amplitude of external applied force (N/m^2).

Table 15 - Convergence of the HFEM linear natural frequencies ω_1. Plate 4.

p_o	3	4	5	6	7
ω_1 (rad/s)	511.577	511.440	511.405	511.390	511.387
ω_2 (rad/s)	646.264	645.576	645.365	645.296	645.281
ω_3 (rad/s)	907.776	903.155	886.902	886.855	886.217

Table 16 - Convergence of frequency ratios ω/ω_1 of the fundamental mode with p_o. Plate 4. $\xi=\eta=0$.

$p_o=3\,p_i=5$		$p_o=4\;p_i=5$		$p_o=5\,p_i=5$		$p_o=6\,p_i=6$	
$\frac{w_{max}}{h}$	ω/ω_1	$\frac{w_{max}}{h}$	ω/ω_1	$\frac{w_{max}}{h}$	ω/ω_1	$\frac{w_{max}}{h}$	ω/ω_1
0.20064	1.0060	0.20930	1.0064	0.19964	1.0059	0.21421	1.0063
0.39990	1.0234	0.39586	1.0229	0.39951	1.0232	0.39765	1.0217
0.59977	1.0519	0.60113	1.0521	0.60012	1.0518	0.60266	1.0495
0.80010	1.0907	0.80035	1.0908	0.79988	1.0904	0.80520	1.0872
1.0000	1.1389	0.99978	1.1389	0.99988	1.1382	0.99661	1.1315
1.2495	1.2106	1.2494	1.2108	1.2499	1.2092	1.2501	1.2018
1.4993	1.2935	1.4992	1.2938	1.5001	1.2904	1.5040	1.2835

Table 17 - Convergence of frequency ratios ω/ω_1 of the second mode with p_o. Plate 4. $\xi= 0.4$, $\eta=0$.

$p_o=3\,p_i=5$		$p_o=4\;p_i=5$		$p_o=5\,p_i=5$		$p_o=6\,p_i=6$	
$\frac{w_{max}}{h}$	ω/ω_1	$\frac{w_{max}}{h}$	ω/ω_1	$\frac{w_{max}}{h}$	ω/ω_1	$\frac{w_{max}}{h}$	ω/ω_1
0.19938	1.2827	0.20010	1.2824	0.20021	1.2820	0.20189	1.2786
0.40007	1.3397	0.40001	1.3399	0.40309	1.3406	0.40413	1.3271
0.59996	1.4297	0.59993	1.4299	0.60258	1.4308	0.59489	1.3978
0.80000	1.5465	0.80021	1.5466	0.79913	1.5457	0.79984	1.4964
1.0001	1.6850	0.99569	1.6814	0.99883	1.6840	0.99869	1.6104
1.2496	1.8812	1.2476	1.8793	1.2500	1.8825	1.2498	1.7752
1.4999	2.0977	1.4999	2.0988	1.4999	2.1006	1.4985	1.9564

Table 18 - Convergence of frequency ratios ω/ω_1 of the third mode with p_o. Plate 4. $\xi = 0, \eta = 0$.

p_o=3 p_i=5		p_o=4 p_i=5		p_o=5 p_i=5		p_o=6 p_i=6	
$\frac{w_{max}}{h}$	ω/ω_1	$\frac{w_{max}}{h}$	ω/ω_1	$\frac{w_{max}}{h}$	ω/ω_1	$\frac{w_{max}}{h}$	ω/ω_1
0.19989	1.8391	0.20072	1.8313	0.19989	1.7971	0.20158	1.7978
0.39903	2.0180	0.39917	2.0046	0.40062	1.9686	0.39868	1.9665
0.60074	2.2674	0.59974	2.2557	0.59964	2.2190	0.59897	2.2192
0.79806	2.5607	0.80000	2.5592	0.80027	2.5332	0.80069	2.5378
1.0000	2.9056	1.0002	2.9024	1.0001	2.8957	0.99887	2.9010
—	—	—	—	1.2500	3.4033	1.2487	3.4133
—	—	—	—	1.4999	3.9556	1.4999	3.9727

Table 19 - Convergence of frequency ratios ω/ω_1 of the fundamental mode. with p_i. Plate 4. p_o=5. $\xi = 0, \eta = 0$.

p_i=0		p_i=3		p_i=4	
$\frac{w_{max}}{h}$	ω/ω_1	$\frac{w_{max}}{h}$	ω/ω_1	$\frac{w_{max}}{h}$	ω/ω_1
0.19985	1.0081	0.19975	1.0076	0.19959	1.0059
0.39984	1.0319	0.39948	1.0301	0.39990	1.0236
0.59991	1.0704	0.60000	1.0667	0.59978	1.0522
0.80003	1.1218	0.80002	1.1156	0.79990	1.0912
1.0000	1.1840	0.99999	1.1753	0.99987	1.1392
1.2526	1.2746	1.2500	1.2618	1.2499	1.21031
1.5012	1.3734	1.4999	1.3583	1.5000	1.2914

p_i=5		p_i=6		p_i=7	
$\frac{w_{max}}{h}$	ω/ω_1	$\frac{w_{max}}{h}$	ω/ω_1	$\frac{w_{max}}{h}$	ω/ω_1
0.19964	1.0059	0.2006	1.0057	0.19992	1.0055
0.39951	1.0232	0.4013	1.0222	0.40364	1.0224
0.60012	1.0518	0.6003	1.0491	0.61101	1.0508
0.79988	1.0904	0.8013	1.0864	0.80613	1.0874
0.99988	1.1382	0.9999	1.1324	0.99977	1.1324
1.2499	1.2092	1.2532	1.2028	1.2531	1.2029
1.5001	1.2904	1.4977	1.2814	1.4976	1.2816

Table 20 - Convergence of frequency ratios ω/ω_1 of the second mode with p_i. Plate 3. p_o=5. $\xi = 0.4$, $\eta = 0$.

p_i=0		p_i=3		p_i=4	
$\frac{w_{max}}{h}$	ω/ω_1	$\frac{w_{max}}{h}$	ω/ω_1	$\frac{w_{max}}{h}$	ω/ω_1
0.19986	1.2848	0.19941	1.2844	0.19979	1.2831
0.39933	1.3503	0.39990	1.3484	0.39942	1.3440
0.59848	1.4516	0.60002	1.4483	0.59895	1.4391
0.79757	1.5816	0.80001	1.5775	0.79865	1.5624
0.99666	1.7346	0.99986	1.7299	1.0015	1.7109
1.2455	1.9501	1.2501	1.9459	1.2496	1.9175
1.5044	2.1953	1.5000	2.1822	1.4994	2.1465

p_i=5		p_i=6		p_i=7	
$\frac{w_{max}}{h}$	ω/ω_1	$\frac{w_{max}}{h}$	ω/ω_1	$\frac{w_{max}}{h}$	ω/ω_1
0.20021	1.2820	0.19988	1.2784	0.20030	1.2781
0.40309	1.3406	0.40009	1.32593	0.39250	1.3224
0.60258	1.4308	0.59970	1.40017	0.60010	1.3981
0.79913	1.5457	0.80099	1.4978	0.79787	1.4930
0.99883	1.6840	0.99935	1.6127	0.99745	1.6076
1.2500	1.8825	1.2500	1.7801	1.2478	1.7732
1.4999	2.1006	1.4999	1.9657	1.5021	1.9611

Table 21 - Convergence of frequency ratios ω/ω_1 of the third mode with p_i. Plate 3. p_o=5. $\xi = 0$, $\eta = 0$.

p_i=0		p_i=3		p_i=4	
$\frac{w_{max}}{h}$	ω/ω_1	$\frac{w_{max}}{h}$	ω/ω_1	$\frac{w_{max}}{h}$	ω/ω_1
0.20004	1.7999	0.19995	1.7974	0.20014	1.7972
0.39979	1.9766	0.39989	1.9705	0.39988	1.9696
0.59902	2.2337	0.60005	2.2261	0.60016	2.2230
0.79799	2.5528	0.79998	2.5439	0.80006	2.5378
1.00192	2.9317	1.0000	2.9111	1.0001	2.9026

p_i=5		p_i=6		p_i=7	
$\frac{w_{max}}{h}$	ω/ω_1	$\frac{w_{max}}{h}$	ω/ω_1	$\frac{w_{max}}{h}$	ω/ω_1
0.19989	1.7971	0.20078	1.7973	0.20094	1.7962
0.40062	1.9686	0.40040	1.9684	0.39886	1.9630
0.59964	2.2190	0.60002	2.2213	0.59930	2.2131
0.80027	2.5332	0.79985	2.5366	0.80077	2.5290
1.0001	2.8957	0.95691	2.8189	1.0004	2.8936
1.2500	3.4033	1.2495	3.4145	1.2494	3.4053
1.4999	3.9556	1.4997	3.9716	1.4983	3.9641

Table 22 - Comparison of frequency ratios ω/ω_1 of the fundamental mode. Plate 3. p_o=5 p_i=5. ξ=η=0.

reference [15]		HFEM and Continuation M.	
$\frac{w_{max}}{h}$	ω/ω_1	$\frac{w_{max}}{h}$	ω/ω_1
0.2	1.0058	0.19964	1.0059
0.4	1.0232	0.39951	1.0232
0.6	1.0516	0.60012	1.0518
0.8	1.0903	0.79988	1.0904
1.0	1.1382	0.99988	1.1382
1.2	1.1941	1.1999	1.1941

FIGURES

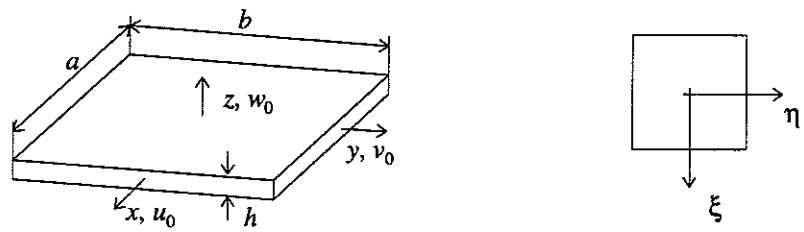

a b

Figure 1 - a) Rectangular plate: x, y and z - global coordinate system; u_0, v_0 and w_0 - middle-plane displacements; a, b and h - length, width and height of plates. b) ξ, η - local coordinate system.

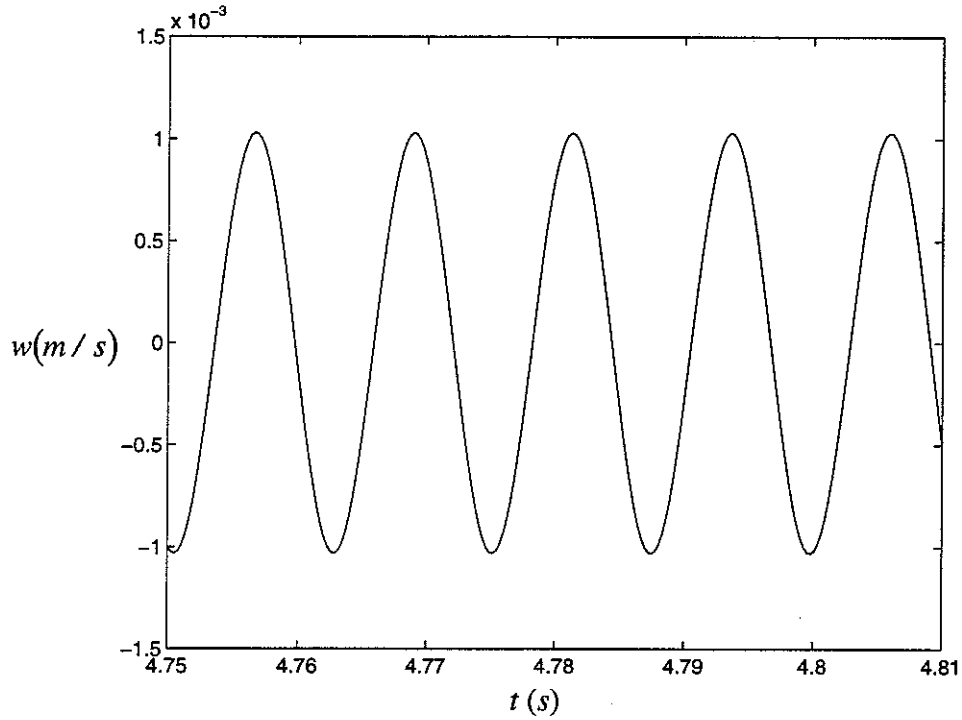

Figure 2 - Time domain response of Plate 4, to an harmonic plane wave, with 510 rad/s frequency.

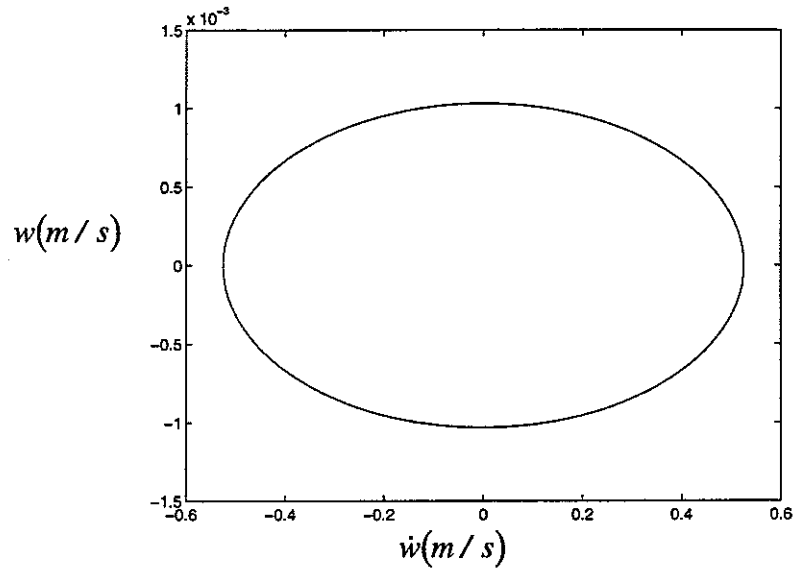

Figure 3 - Phase plane of the steady-state vibration of Plate 4 due to an excitation by an harmonic plane wave, with 510 rad/s frequency. Note that a closed path in the phase plane is characteristic of a periodic motion.

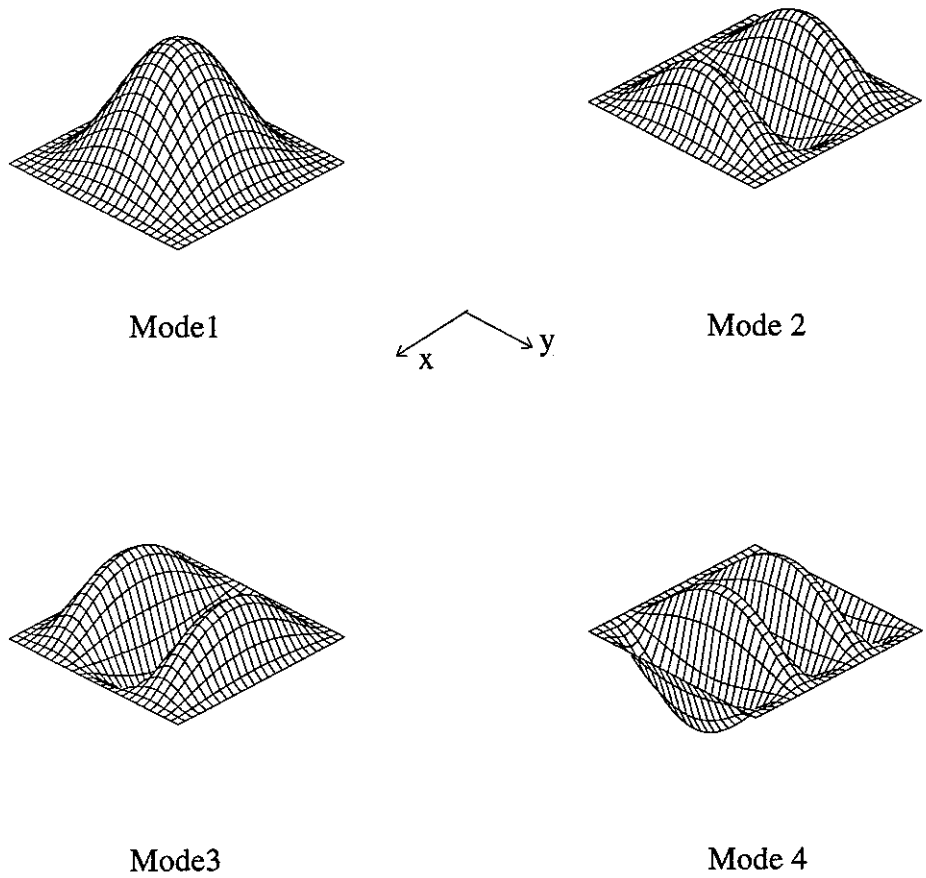

Figure 4 - First four bi-symmetric linear modes of vibration of Plate 1. p_o=5.

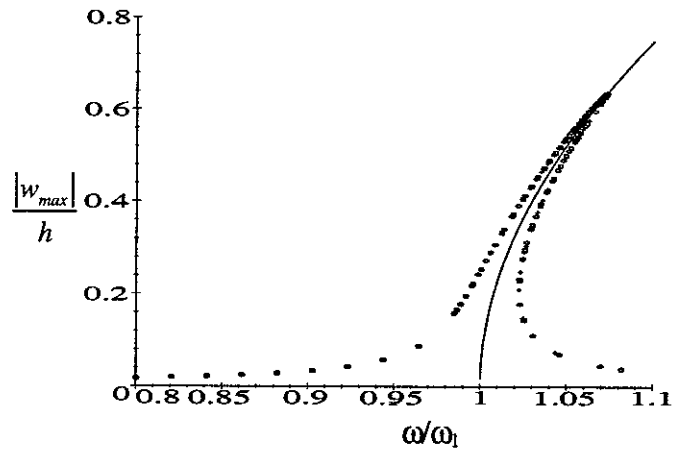

Figure 5 - Convergence with p_o in the vicinity of the first mode. FRFs:□ p_o = 2, o p_o = 3, + p_o = 4; Backbone curves: — ω_1 - first linear frequency.

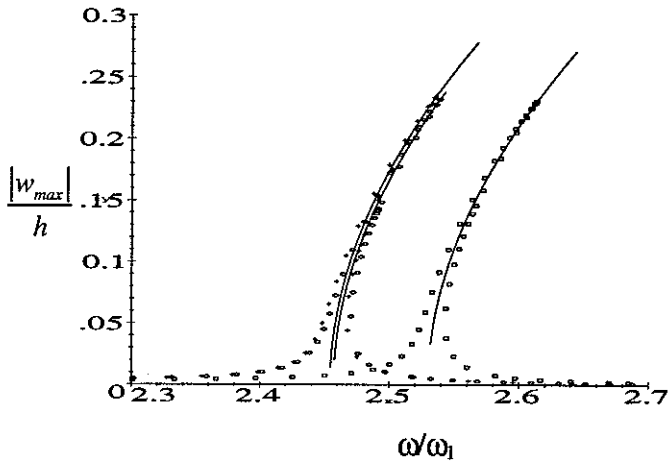

Figure 6 - Convergence with p_o in the vicinity of the second mode. Legend as in Fig. 5.

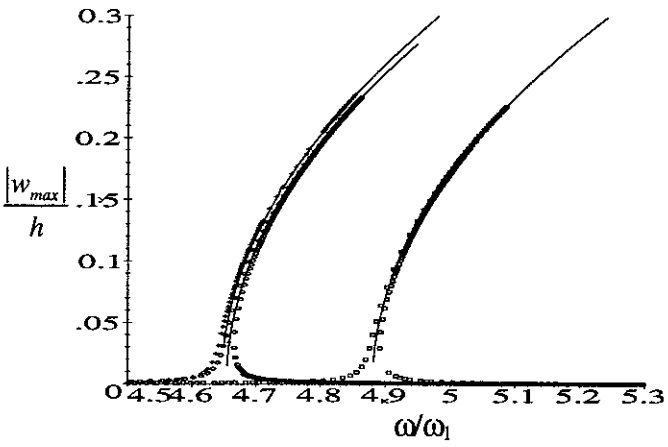

Figure 7 - Convergence with p_o in the vicinity of the third mode. Legend as in Figure 5.

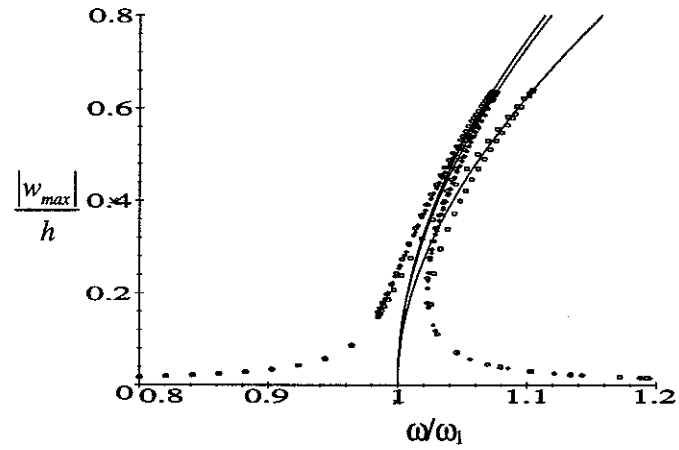

Figure 8 - Convergence with p_i in the vicinity of the first mode. FRFs:□ p_i = 0, + p_i = 4, ◊ p_i = 5, o p_i=6; Backbone curves: —.

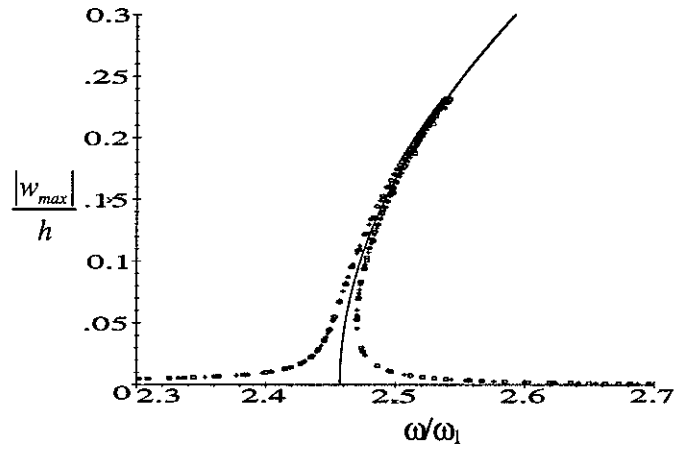

Figure 9 - Convergence with p_i in the vicinity of the second mode. FRFs:□ p_i = 0, + p_i = 3, ◊ p_i = 4, o p_i=5; Backbone curves: —.

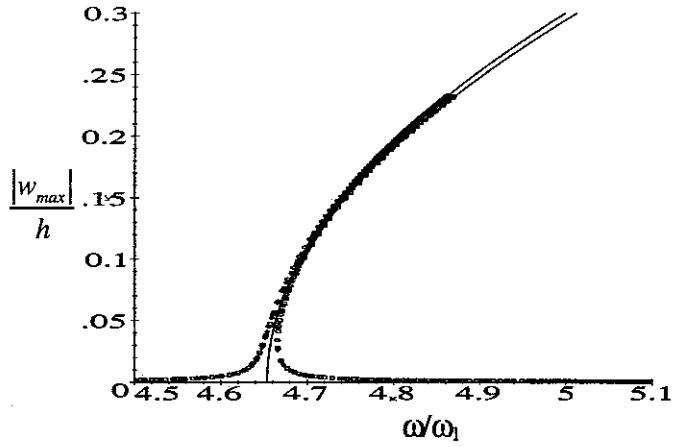

Figure 10 - Convergence with p_i in the vicinity of the third mode. Legend as in Fig. 9.

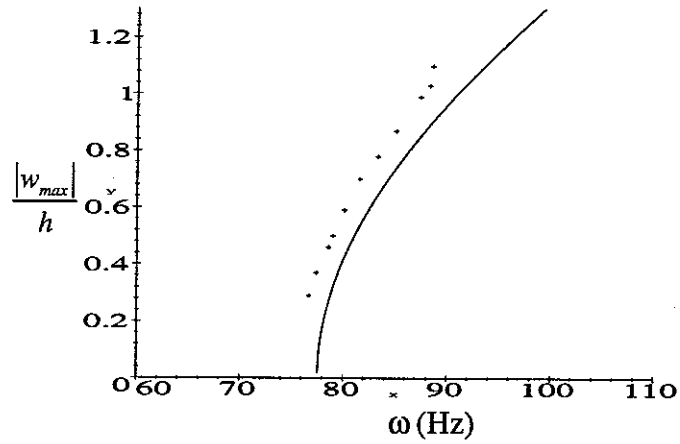

Figure 11 - Comparison between the first resonance frequency predicted by the HFEM, —, and the measured one, + (Benamar, 1990).

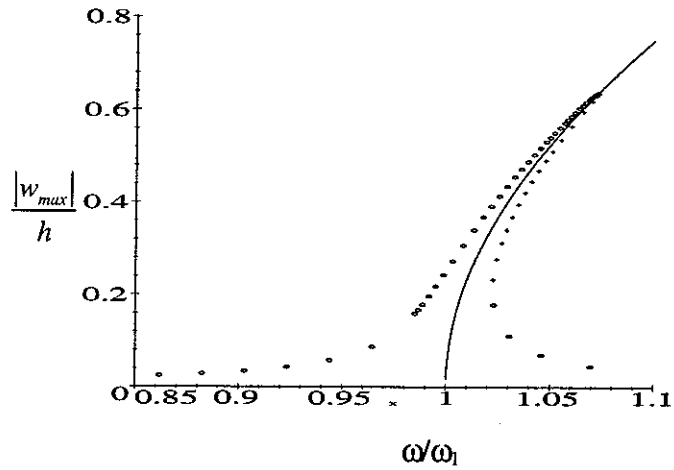

Figure 12 - Stability study in the vicinity of the first mode. o stable solutions, + unstable solutions.

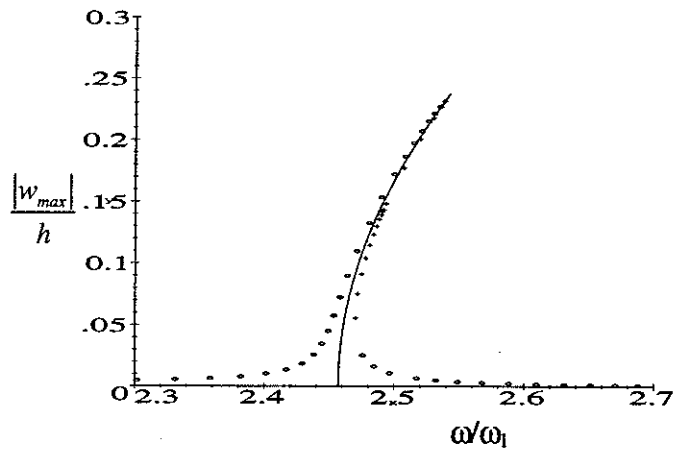

Figure 13 - Stability study in the vicinity of the second mode. Legend as in Figure 12.

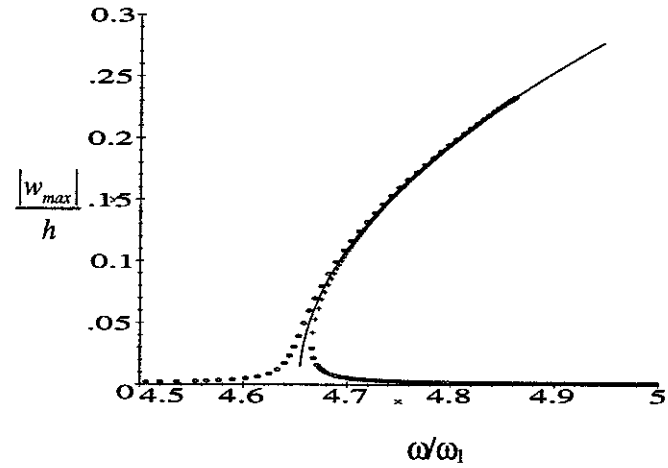

Figure 14 - Stability study in the vicinity of the third mode. Legend as in Figure 12.

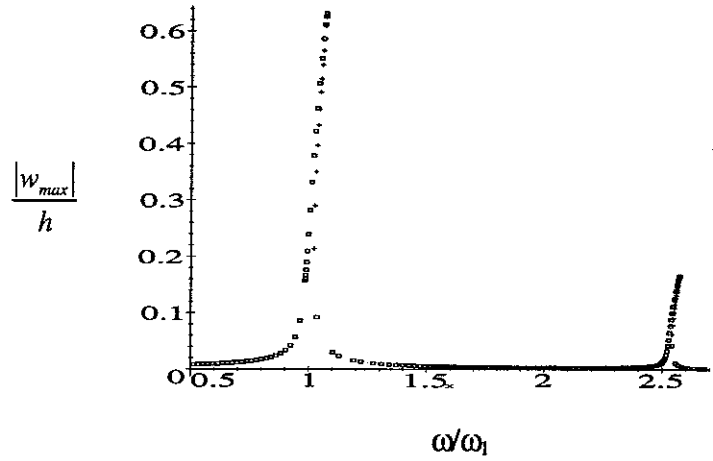

Figure 15 - Response to an harmonic plane wave at grazing incidence, p_o=4, p_i=6 and P_g=10 N/m^2. o stable solutions, + unstable solutions. ξ=η=0.

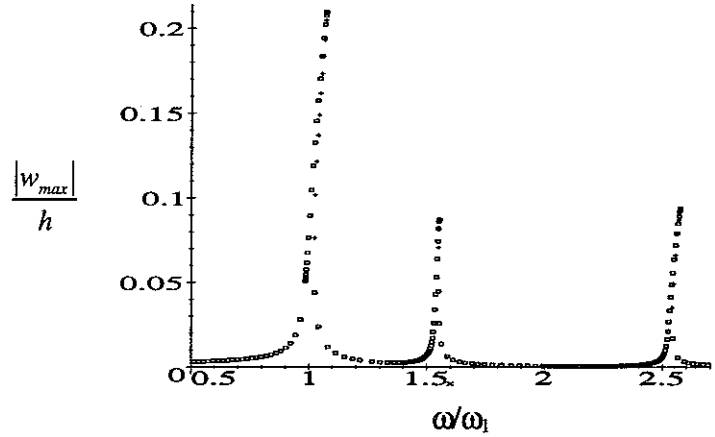

Figure 16 - Response to an harmonic plane wave at grazing incidence, p_o=4, p_i=6 and P_g=10 N/m^2. o stable solutions, + unstable solutions. ξ=η=0.5.

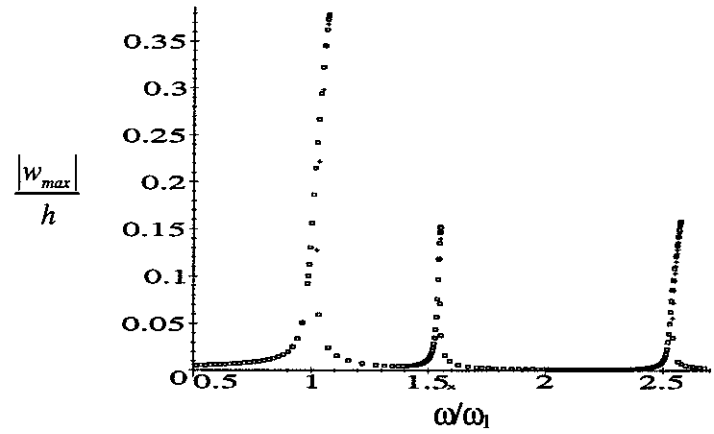

Figure 17 - Response to an harmonic plane wave at grazing incidence, p_o=4, p_i=6 and P_g =10 N/m^2. o stable solutions, + unstable solutions. ξ=0.5, η=0.

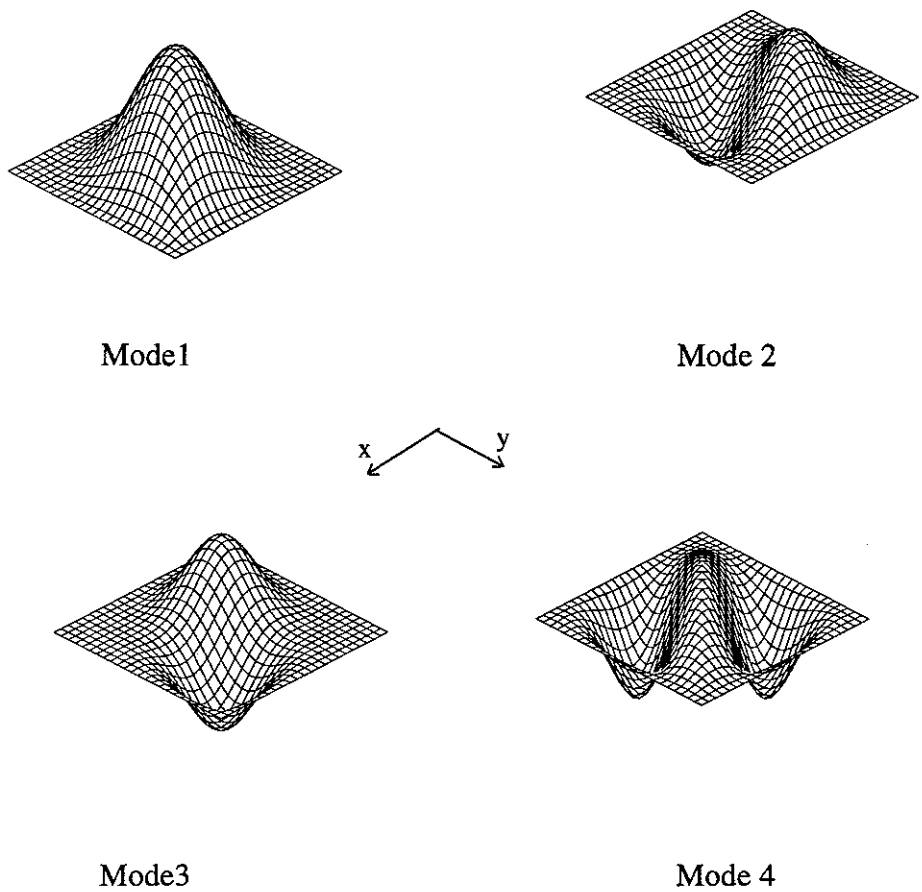

Figure 18 - First four linear modes of vibration of Plate 3. p_o=5.

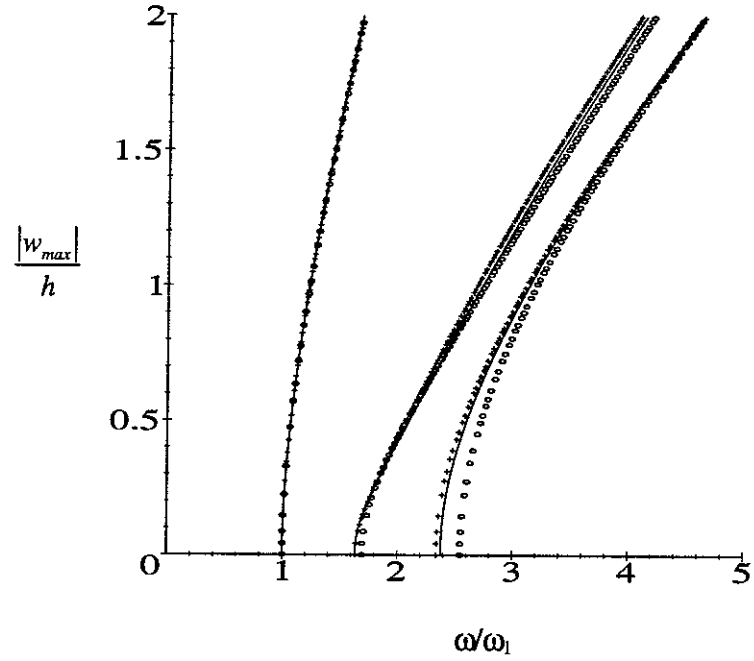

Figure 19 - Convergence in free vibration with p_o for the first three modes of Plate 3. $p_i = 5$; o $p_o = 3$, — $p_o = 4$, + $p_o = 5$.

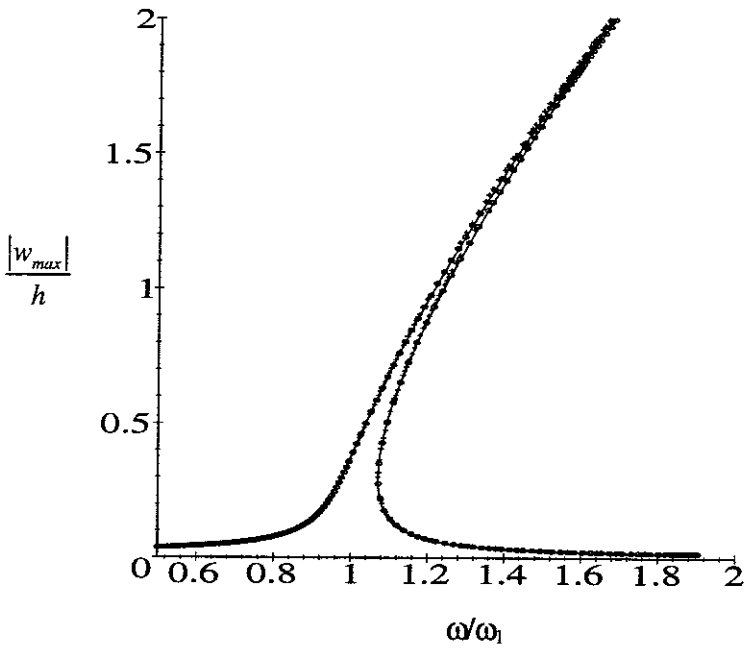

Figure 20 - Convergence in forced vibration with p_o around the first mode. Plate 3. P_d=1000 N/m^2. $p_i = 5$;+ $p_o = 3$,— $p_o = 4$ and ∘ $p_o = 5$.

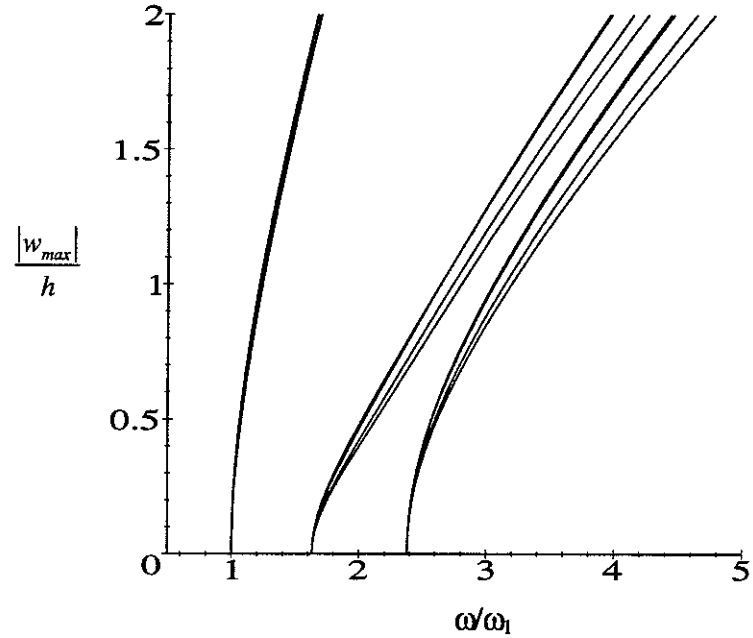

Figure 21 - Convergence in free vibration with p_i for Plate 3. $p_o = 4$; in each mode from right to left: $p_i = 4$, $p_i = 5$, $p_i = 6$, $p_i = 7$. First mode calculated at $\xi=\eta=0$, second at $\xi=0.4$, $\eta=-0.4$ and third at $\xi=0.4, \eta= 0.4$.

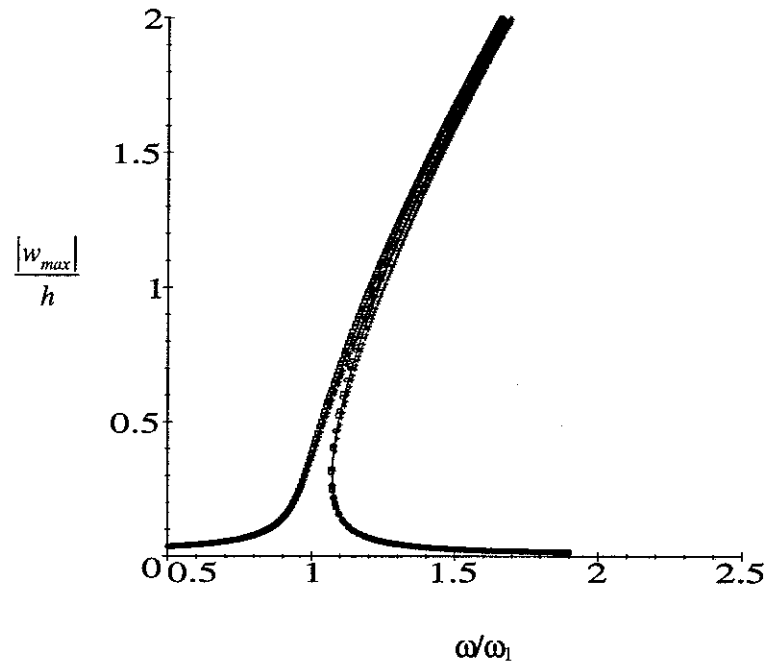

Figure 22 - Convergence in forced vibration around the first mode. Plate 3. P_d=1000 N/m^2. $p_o = 4$; + $p_i = 4$, — $p_i = 5$, ∘ $p_i = 6$, □ $p_i = 7$.

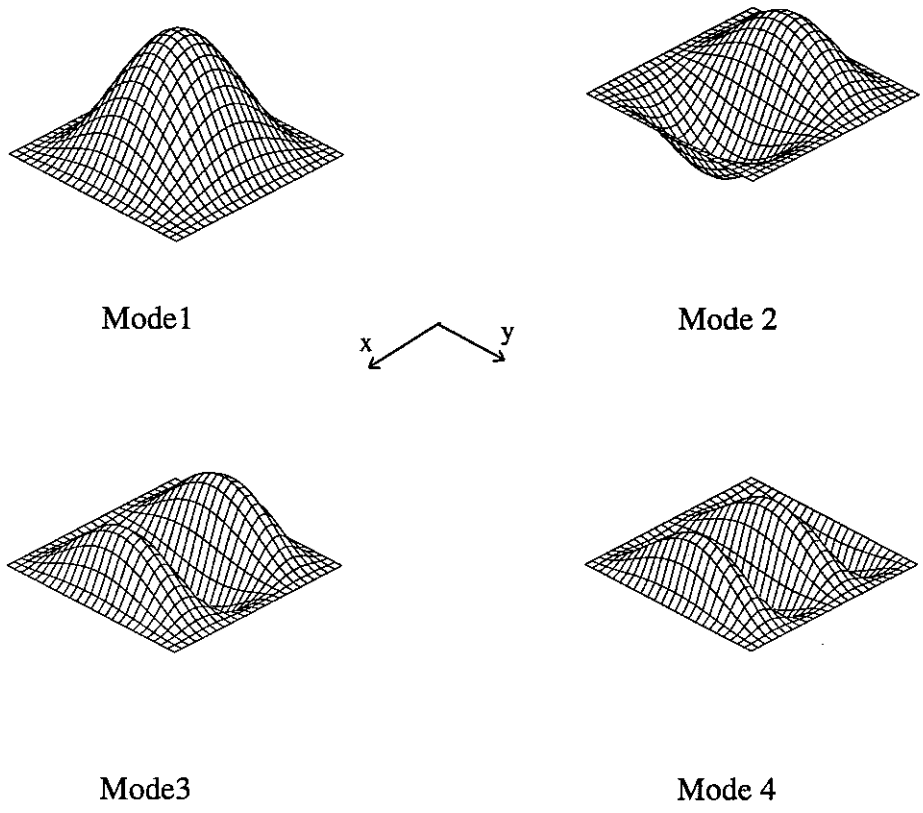

Figure 23 - First four linear modes of vibration of Plate 4. p_o=6.

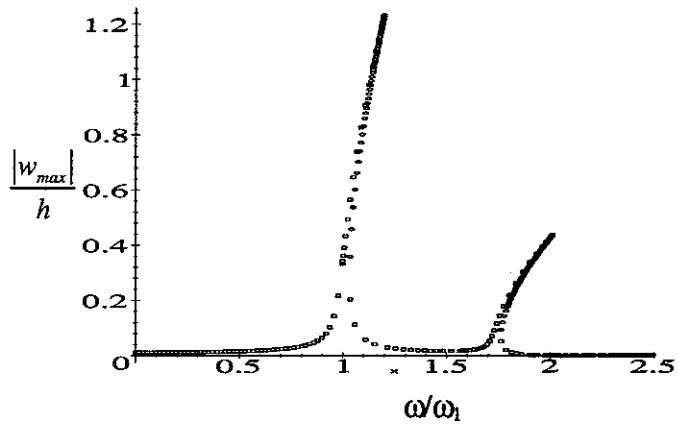

Figure 24 - Response to an harmonic plane wave at normal incidence, p_o=5, p_i=6 and P_d=3 N/m^2. □ stable solutions, o unstable solutions. ξ=η=0. Plate 4.

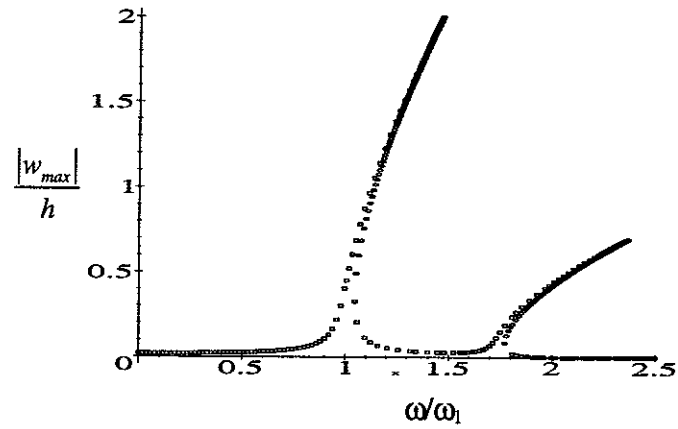

Figure 25 - Response to an harmonic plane wave at normal incidence, p_o=5, p_i=6 and P_d=5 N/m^2.□ stable solutions, o unstable solutions. ξ=η=0. Plate 4.

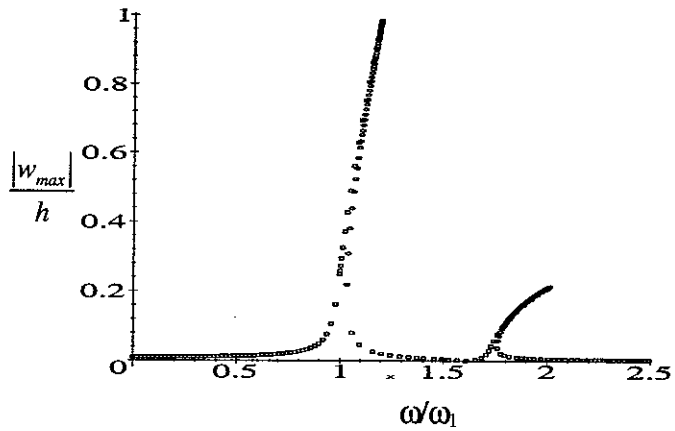

Figure 26 - Response to an harmonic plane wave at normal incidence, p_o=5, p_i=6 and P_d=3 N/m^2. □ stable solutions, o unstable solutions. ξ=0.4, η=0. Plate 4.

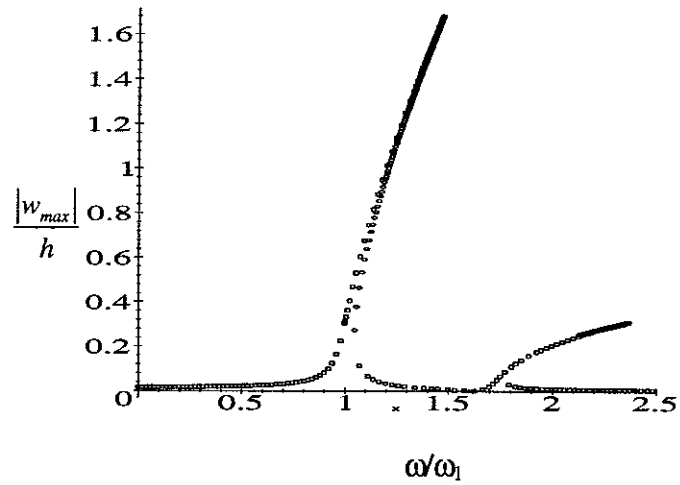

Figure 27 - Response to an harmonic plane wave at normal incidence, p_o=5, p_i=6 and P_d=5 N/m^2. □ stable solutions, o unstable solutions. ξ=0.4, η=0. Plate 4.

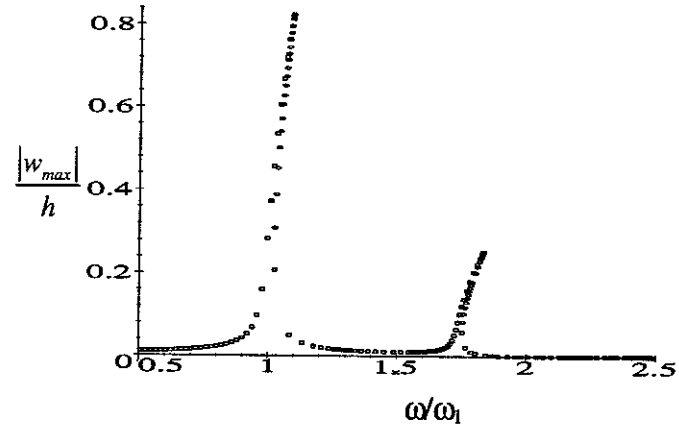

Figure 28 - Response to an harmonic plane wave at grazing incidence, $\alpha=0^{o}$, p_o=5, p_i=6 and P_g=2 N/m^2. □ stable solutions, o unstable solutions. ξ=0, η=0. Plate 4.

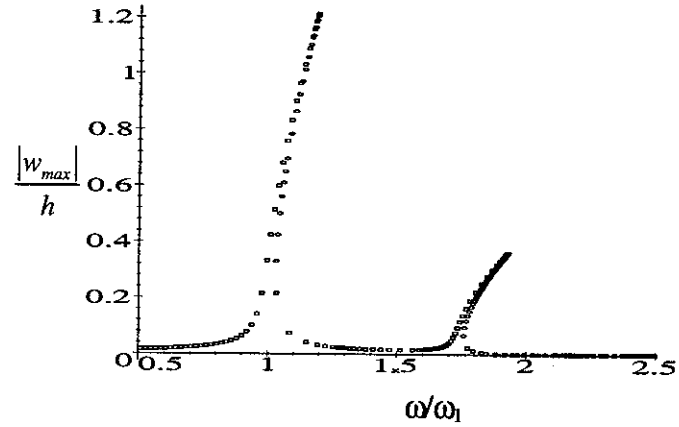

Figure 29 - Response to an harmonic plane wave at grazing incidence, $\alpha=0^{o}$, p_o=5, pi=6 and P_g=3 N/m^2. □ stable solutions, o unstable solutions. ξ=0, η=0. Plate 4.

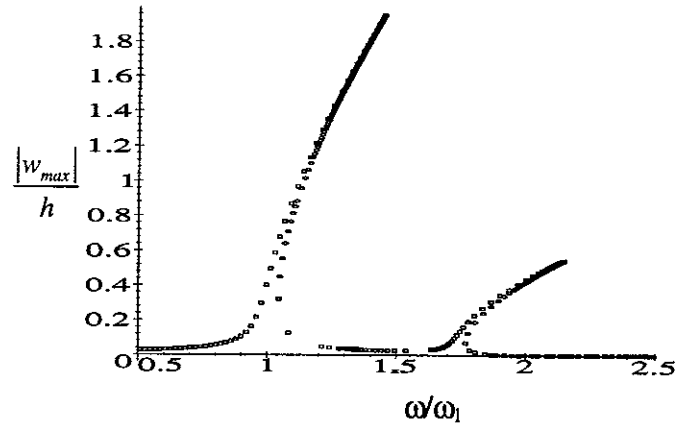

Figure 30 - Response to an harmonic plane wave at grazing incidence, $\alpha=0^{o}$, p_o=5, p_i=6 and P_g =5 N/m^2.□ stable solutions, o unstable solutions. ξ=0, η=0. Plate 4.

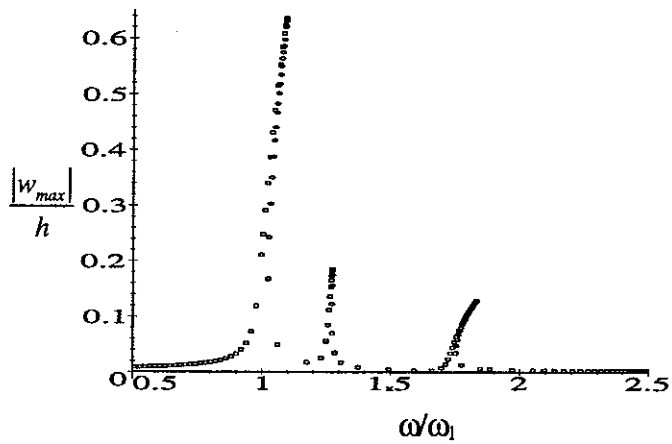

Figure 31 - Response to an harmonic plane wave at grazing incidence, $\alpha=0^o$, p_o=5, p_i=6 and P_g =2 N/m^2. □ stable solutions, o unstable solutions. ξ=0.4, η=0 .

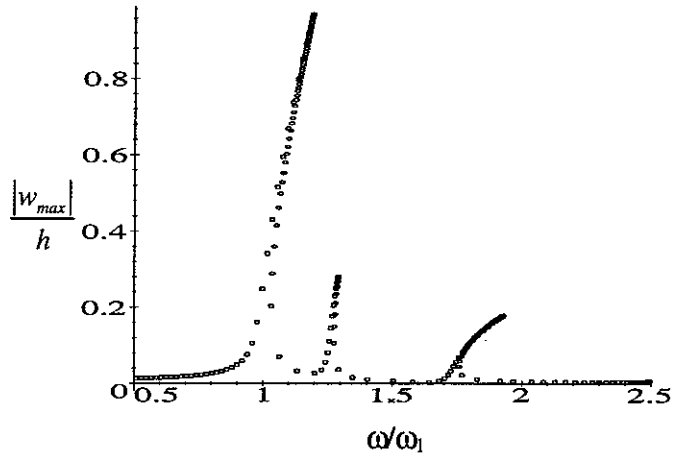

Figure 32 - Response to an harmonic plane wave at grazing incidence, $\alpha=0^o$, p_o=5, p_i=6 and P_g =3 N/m^2. □ stable solutions, o unstable solutions. ξ=0.4, η=0 .

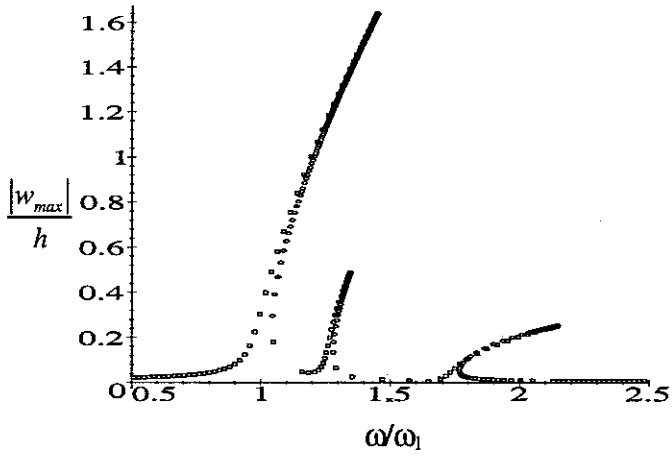

Figure 33 - Response to an harmonic plane wave at grazing incidence, $\alpha=0^o$, p_o=5, p_i=6 and P_g =5 N/m^2. □ stable solutions, o unstable solutions. ξ=0.4, η=0 .